

Exhibit 47


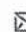
ScienceDirect[®]


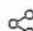


Heliyon

Volume 10, Issue 1, 15 January 2024, e23968

Review article

Ni-rich lithium nickel manganese cobalt oxide cathode materials: A review on the synthesis methods and their electrochemical performances

Farish Irfal Saaid^{a c}, Muhd Firdaus Kasim^{a b}  , Tan Winie^{a c}, Kelimah Anak Elong^{a b}, Azira Azahidi^a, Nurul Dhabitah Basri^{a b}, Muhamad Kamil Yaakob^{a c}, Mohd Sufri Mastuli^{a b}, Siti Nur Amira Shaffee^d, Mohd Zaid Zolkiffly^d, Mohamad Rusop Mahmood^a

Show more  Outline |  Share  Cite<https://doi.org/10.1016/j.heliyon.2023.e23968> [Get rights and content](#) [Under a Creative Commons license](#)  open access

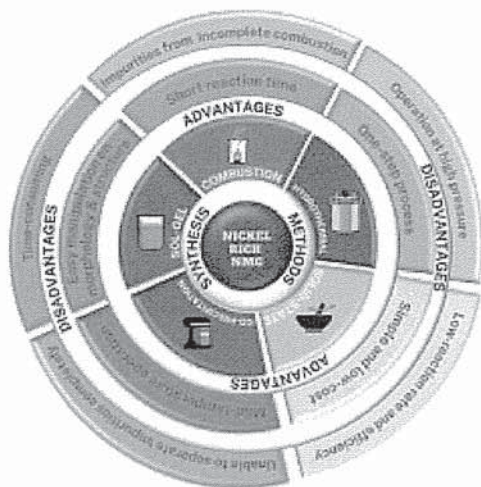
Abstract

The demand for lithium-ion batteries (LIBs) has skyrocketed due to the fast-growing global electric vehicle (EV) market. The Ni-rich cathode materials are considered the most relevant next-generation positive-electrode materials for LIBs as they offer low cost and high energy density materials. However, by increasing Ni content in the cathode materials, the materials suffer from poor cycle ability, rate capability and thermal stability. Therefore, this review article focuses on recent advances in the controlled synthesis of lithium nickel manganese cobalt oxide (NMC). This work highlights the advantages and challenges associated with each synthesis method that has been used to produce Ni-rich materials. The crystallography

Case 2:24-cv-10546-BRM-KGA ECF No. 30-48, PageID.4719 Filed 11/25/24 Page 3 of 69

and morphology obtained are discussed, as the performance of LIBs is highly dependent on these properties. To address the drawbacks of Ni-rich cathode materials, certain modifications such as ion doping, and surface coating have been pursued. The correlation between the synthesized and modified NMC materials with their electrochemical performances is summarized. Several gaps, challenges and guidelines are elucidated here in order to provide insights for facilitating research in high-performance cathode for lithium-ion batteries. Factors that govern the formation of nickel-rich layered cathode such as pH, reaction and calcination temperatures have been outlined and discussed.

Graphical abstract



Download : Download high-res image (391KB)

Download : Download full-size image



Previous

Next



Keywords

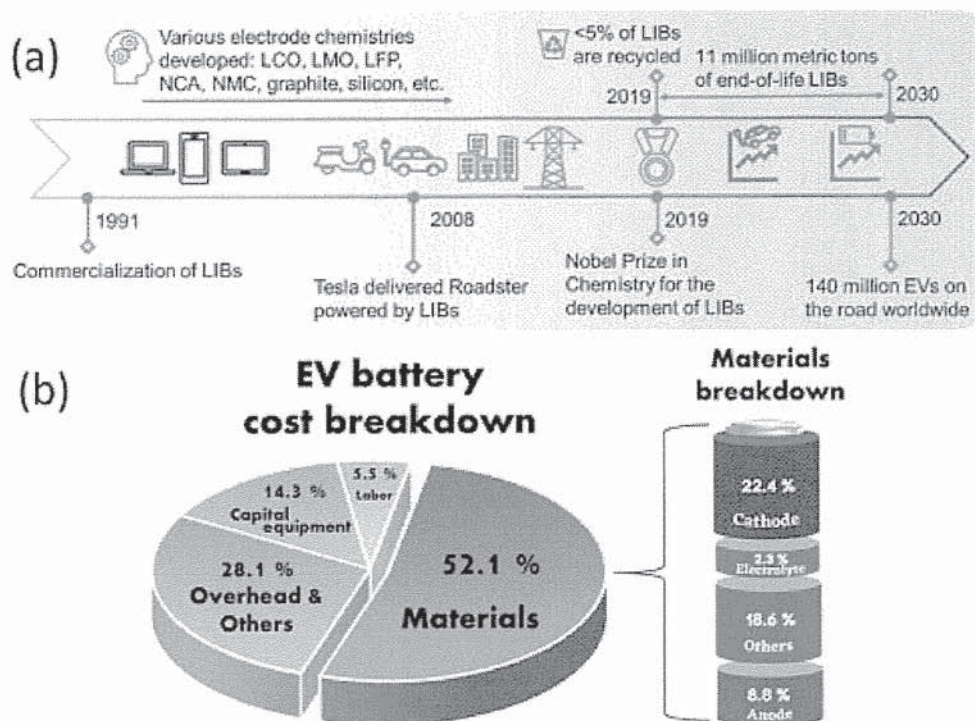
Synthesis; Nickel-rich cathode; NMC; Electrochemical performance; Lithium-ion batteries

1. Introduction

A massive revolution in world's advanced technologies has been surging from one niche step to superior achievement in many sectors including the future of road transportation. In 1880s, the first electric vehicle (EV) was invented by an automaker in Des Moines with a

capability of travelling 14 miles per hour competing with the conventional car; this then appeared to be the propulsion of automotive evolution in developing the EV range. This EV era is exceptionally growing from time to time because subsequent researchers and the development of automotive interests such as Tesla and other industrial experts believe that such inventions may essentially contribute to economic and environmental values. This era is expected to be dominantly leading the global share of road transport by 11–28% by 2040 based on previous annual EV sales that hit over 753 thousand in 10 years [1,2]. The good values that prompted the acceleration in fabricating high-performance EVs, could be the economic and environmental values like minimal fuel use, alleviation in total carbon emission or clean-energy vehicle models, no emission of greenhouse gases as well as reduction of fossil fuel dependent. Therefore, many European countries, USA, China, and Japan have already made a few strategic moves to promote EVs such as purchase rebates, tax exemptions, and tax credits [3].

Generally, commercial EVs are powered by a compact rechargeable battery pack that holds thousands of lithium-ion batteries (LIBs). This battery pack is charged by simply plugging in the EVs at a charging point. The stored charge is then used to power the electric motor and other electrical components. Since their first commercialization in 1990s, LIBs are widely used in most portable electronic devices such as drones, mobile phones, and laptops; now they are the frontrunner in powering EVs (cf. Fig. 1(a)). This is because LIBs have advantages in size and weight as compared to large and heavy lead-acid batteries or nickel-cadmium batteries. Therefore, LIBs are drawing interests from many researchers due to their attractive features such as rechargeability, high specific energy and power density, and long cycle life [4]. However, LIBs are expensive as they utilize scarce metals such as lithium and cobalt. These metals need to be mined and processed into high-purity chemical compounds prior to use. This has hit a high price tag on EVs, as they rely on huge mineral-intensive LIBs to power the automobiles [5].

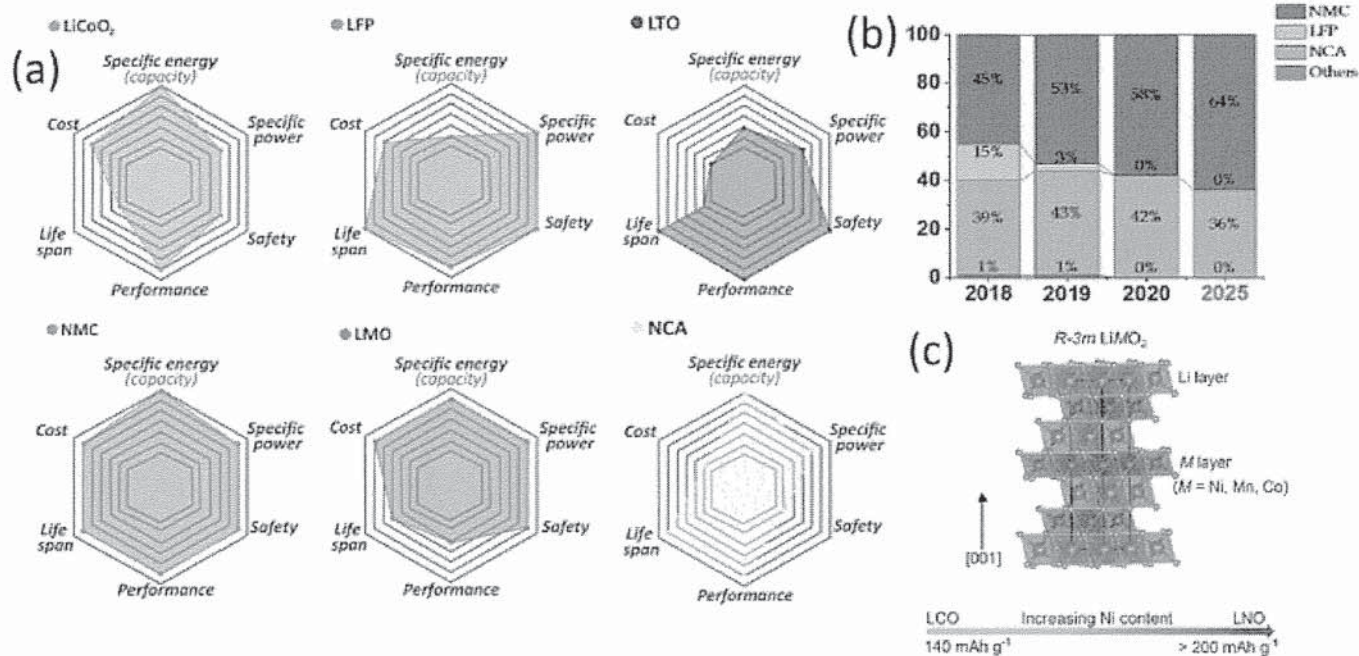


Download : Download high-res image (513KB)

Download : Download full-size image

Fig. 1. (a) The past and present applications of LIBs and future application projection of LIBs. Reprinted with permission from Ref. [8], Copyright 2021 Elsevier. (b) EVs battery cost breakdown [9].

LIBs are made up of four main components: anode, cathode, separator, and electrolyte. Among these components, the cathode currently acts as a limiting factor that controls a large degree of the operation voltage and storage capacity [6]. The cathode also dominates the battery cost by 22.4 % as this is where most of the scarce metals are sited (cf. Fig. 1(b)). Hence, the development of high-performance with low-cost cathodes is necessary to reduce the cost of LIBs. There has been extensive research on cathode materials such as lithium cobalt oxide (LCO), lithium iron phosphate (LFP), lithium-titanate (LTO), lithium manganese oxide (LMO), and recently, lithium nickel cobalt aluminium oxides (NCA) and lithium nickel manganese cobalt oxide (NMC). Fig. 2(a) compares the cost, lifespan, performance, safety, specific energy, and power of these cathode materials. Among all, the NMC has the best all-around performance. Due to its advantages, the NMC battery is gaining popularity in the global LIBs market. According to Bloomberg New Energy Finance, NMC battery adoption rate in EVs battery market constantly increases over the year and it is expected to reach 64% in 2025 (cf. Fig. 2(b)) [7].



Download : Download high-res image (688KB)

Download : Download full-size image

Fig. 2. (a) Comparison of different types of cathodes [16], (b) adoption rate per chemistry in EV battery market [16] and (c) crystal structure of R-3m LiMO₂ layered oxide (M=Ni, Co, and Mn). Reprinted with permission from Ref. [12], Copyright 2021 AIP Publishing.

Layered cathode materials are comprised of nickel, manganese, and cobalt elements and known as NMC or LiNi_xMn_yCo_zO₂ (x+y+z=1). NMC has been widely used due to its low cost, environmental benign and more specific capacity than LCO systems [10]. Combination of Ni, Mn and Co elements in NMC crystal structure, as shown in Fig. 2(c)–is reported to have a good structural stability up to 60% Ni content while minimizing Co content [11]. In NMC crystal structure, the redox behaviour of Ni²⁺ to Ni⁴⁺ governs the electrochemical activity, whereas the electrochemical inactive Mn⁴⁺ takes charge in structural stabilization [12]. On the one hand, Co can enhance the electronic conductivity and suppress the Li/Ni mixing in the Ni-rich layered cathodes [[13], [14], [15]], thereby increase the rate capability and the specific capacity.

NMC is widely applied in EV system as it delivers higher discharge capacity and greater mile-range per charge as shown in Table 1. Besides stabilizing the material structure, Co also allows a superior diffusion rate of Li-ion which benefits the electrochemical performance of the batteries. The diversity in NMC materials is because of the different composition of nickel, cobalt, and manganese, forming LiNi_{1/3}Mn_{1/3}Co_{1/3}O₂ (NMC333), LiNi_{0.4}Co_{0.4}Mn_{0.2}O₂ (NMC442), LiNi_{0.5}Mn_{0.3}Co_{0.2}O₂ (NMC532), LiNi_{0.6}Mn_{0.2}Co_{0.2}O₂ (NMC622), and LiNi_{0.8}Mn_{0.1}Co_{0.1}O₂ (NMC811) [15,17]. The first commercialized NMC333, was not capable to

meet the demand in EVs application. Thus, modification is done by increasing the Ni content that resulted in increased capacity and rate performance as well as enhanced lifetime. However, this Ni-rich material adoption must be investigated thoroughly because exaggerating Ni content (>60%) may cause capacity fading, severe surface reactivity and structural uncertainty which eventually lead to deterioration of performances.

Table 1. NMC cathodes used in EVs and their main characteristics [16,19].

Cathode Type	Ratios (R) or Cell Designation (S)	Manufacturer	No of Cells (Series Parallel)	EV Model	Specific Energy (Wh kg ⁻¹)	Energy (Useable) (kWh)	Range* (km)
Li-Nickel Manganese Cobalt Oxide	532 (R)	Nissan	288	Nissan Leaf e+	–	62	385
		CATL	216 (s108p2)	Peugeot e-208, Opel Corsa-e	140	50 (46)	349, 336
		Envision AESC	192 (s96p2)	Nissan Leaf	130	39.5 (36)	270
	333 (R)	Samsung SDI	246 (s88p3)	Volkswagen e-Golf	103	35.8 (32)	232
	721 (R)	LG Chem	192 (s96p2)	Renault ZOE	168	54.7 (52)	232
		SK Innovation	288 (s96p3)	Volkswagen ID.4 Pro	–	82 (77)	467
	622 (R)	Samsung SDI	96 (s96p1)	BMW i3	152	42.2 (37.9)	293
		SK Innovation	294 (s98p3)	Kia e-Soul, Kia e-Niro	148	67.5 (64)	451, 454
			168 (s84p2)	Volkswagen e-UP, Seat Mii Electric, Skoda CITIGo-e	148	36.8 (32.3)	260, 256, 265


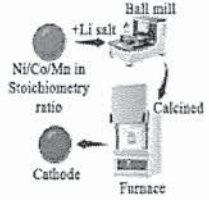
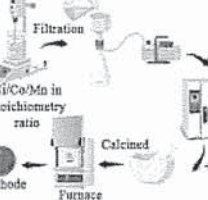


Cathode Type	Ratios (R) or Cell Designation (S)	Manufacturer	No of Cells (Series Parallel)	EV Model	Specific Energy (Wh kg ⁻¹)	Energy (Useable) (kWh)	Range* (km)
			176 (s88p2)	Hyundai Ioniq-e	112.4	40.4 (38.3)	310
			294 (s98p3)	Hyundai Kons-e	149	67.5 (64)	447
			384 (s96p4)	Mercedes Benz EQC	130	85 (80)	417
		LG Chem	396 (s198p2)	Porche Taycan, Jaguar I-Pace	148, 149	93.4 (83.7), 90 (84.7)	333 470
			432 (s108p4)	Audi e-tron 55 Quattro	136	95 (86.5)	402
			288 (s96p3)	Chevrolet Bolt	143	68	417
	811(R)	–	102 (102s1p)	Jeep Avenger	–	54 (50.8)	346
				Vauxhall Astra Sports Tourer			346
				DS 3E-Tense			346

There are various methods to synthesize NMC such as sol-gel, co-precipitation, solid-state, hydrothermal, and combustion methods. Table 2 summarizes the advantages and disadvantages of each method. These methods have been reported to have good control over the chemical composition and particle properties such as crystallinity, microstructure, and surface functionality, which greatly influence the battery performance [18]. Choosing a suitable synthesis method for producing Ni-rich NMC cathode materials is crucial due to several key factors such as capacity and energy density, cycle life and stability, thermal stability and safety, that directly could influence the performance and safety of lithium-ion batteries. For instance, the synthesis method can affect the crystal structure, particle size, and morphology of NMC cathode materials. The capacity, energy density, power density and

Case 2:24-cv-10546-BRM-KGA ECF No. 30-48, PageID.4725 Filed 11/25/24 Page 9 of 69

cycle life of battery are governed by these characteristics to a certain extent. A suitable synthesis method can help achieve the desired balance between these properties and optimize the overall battery performance. Ni-rich NMC cathode materials offer high energy density due to their high nickel content. However, improper synthesis methods can lead to structural defects, phase impurities, or uneven distribution of elements, which can reduce the overall capacity and energy density of the battery. Ni-rich NMC cathode materials are known to be susceptible to certain safety issues, such as thermal runaway and the risk of triggering battery fires. Proper synthesis methods can help mitigate these risks by ensuring uniformity and minimize the presence of impurities or defects that could trigger unwanted reactions under stressful conditions. The synthesis method also can affect the uniformity of particle size, composition, and crystal structure within the cathode material. Inconsistent properties can lead to uneven performance across different parts of the battery, resulting in reduced overall efficiency and reliability. It is important to note that when choosing a synthesis method, factors such as economical, simplicity, and toxicity of the synthesis procedures, and the reproducibility of the synthesis product have to be considered. This article provides a review on alteration of Ni-rich NMC with respect to synthesis condition. Correlations between their microstructure and electrochemical performance are also reported.

Table 2. A comparison of various synthesis methods.

Methods				
Sol-Gel Method	Solid-State method	Co-precipitation	Hydrothermal	Combustion
				
Advantages <ol style="list-style-type: none"> 1. Simple and low-cost 2. Easy manipulation of morphological and microstructure 	Advantages <ol style="list-style-type: none"> 1. Simple and low-cost 2. Product purification can be done by filtration 3. Less solvent used 4. Environmental-friendly 	Advantages <ol style="list-style-type: none"> 1. Spherical morphology particles 2. Good structural homogeneity at the atomic level 3. High tap density 4. Low temperature operation 	Advantages <ol style="list-style-type: none"> 1. Produce fine crystalline phase 2. One-step synthetic procedure 3. Effective in controlling the crystal composition 	Advantages <ol style="list-style-type: none"> 1. Low cost with simple equipment 2. Short reaction time
Disadvantages <ol style="list-style-type: none"> 1. Time-consuming 2. Presence of residual 3. Micron particles size 	Disadvantages <ol style="list-style-type: none"> 1. Powder is not fine enough 2. Low reaction rates and efficiency 3. High tendency of Li vaporization 	Disadvantages <ol style="list-style-type: none"> 1. Unable to separate impurities from the product completely 2. Reactants must have almost similar precipitant rates 	Disadvantages <ol style="list-style-type: none"> 1. High cost for a set of autoclaves 2. Hard to observe the reaction process from the autoclave body 3. Operation at high pressure and reaction temperature 	Disadvantages <ol style="list-style-type: none"> 1. Vigorous method 2. Organic impurities residues from incomplete combustion 3. Low yield

2. Synthesis and electrochemical performance of Ni-rich NMC

The electrochemical performance of cathode materials is dependent on their intrinsic nature properties such as their chemical composition and particle properties [20]. The cathode material namely NMC has various chemical compositions with different combinations of nickel, manganese, and cobalt elements. The tuning of the transition-metal compositions of NMC by reducing the cobalt content has become a headline in the battery field, especially in the effort to optimize desirable battery properties while reducing cost and toxicity [21]. The transition-metal composition of the synthesized NMC can be controlled by varying the stoichiometric ratio of the metal-salt precursor at the early stage of the synthesis process. On the other hand, the particle properties like crystallinity, microstructure, and surface functionality of the synthesized cathode materials may vary significantly with the selection of the synthesis methods, parameters, and conditions [20]. Table 3 lists some reported works on NMC622 and NMC811, synthesized using different methods and their electrochemical performances. As seen in Table 3, most of the NMC622 cathode materials obtained lower initial discharge capacity as compared to NMC811. This implies that tuning the chemical composition with higher Ni content improved the specific capacity of LIBs.

Table 3. NMC622 and NMC811 synthesized using different methods and their electrochemical performances.

Ni-rich NMC	Synthesis Route	Current density	Voltage range (V)	Initial discharge capacity (mAh g ⁻¹)	Cycle no.	Final discharge capacity (mAh g ⁻¹)	Capacity retention	References
NMC622	Solid state reaction	0.5C	2.8–4.3	153.8	100	152.4	99.1%	[22]
	Solid state reaction	1.0C	2.8–4.3	160.8	40	150.6	93.7 %	[23]
	Co-precipitation	0.05C	3.0–4.3	210.0	100	197.4	94.0 %	[24]
	Hydrothermal	0.5C	2.8–4.6	185 .0	50	149.9	81.0 %	[25]
	Combustion	1.0C	2.8–4.3	170.0	30	166.9	98.2 %	[26]
NMC811	Sol-gel	0.5C	2.5–4.3	200.0	50	164.4	82.2%	[27]

Ni-rich NMC	Synthesis Route	Current density	Voltage range (V)	Initial discharge capacity (mAh g ⁻¹)	Cycle no.	Final discharge capacity (mAh g ⁻¹)	Capacity retention	References
	Sol-gel	1.0C	2.7–4.3	176.3	100	139.3	79.0 %	[28]
	Solid State Reaction	2.0C	2.8–4.3	125.2	500	13.7	10.9 %	[29]
	Hydrothermal	1.0C	2.8–4.3	190.0	200	163.8	86.2 %	[30]
	Co-precipitation	1.0C	3.0–4.3	172.0	100	126.6	73.6 %	[31]
	Co-precipitation	0.2C	2.8–4.3	188.7	184	150.9	80 %	[32]

However, further addition of Ni more than the optimum amount may cause NMC to suffer from high-capacity fading, as well as poor structural and thermal stability which will result in quick cell failure [21,33]. These degradation mechanisms are due to a variety of factors [[34], [35], [36], [37]]: (1) Ni²⁺ mixing with the Li⁺ sites due to the similar ionic radius which can hinder lithium diffusion, (2) unfavourable side reactions with the electrolyte and ambient air, which consume both the electrode and electrolyte, (3) volume change during cycling followed by the formation of microcracks. However, these unwanted factors can be restrained with thin surface coating and ion doping methods [38]. A coating mainly provides surface protection to the materials from outside, while ion doping modifies the internal structure of the materials [34]. Table 4 tabulates some modifications made onto NMC622 and NMC811 via doping and coating techniques, that have further enhanced the electrochemical performance of Ni-rich LIBs.

Table 4. Modification of NMC622 and NMC811 and their electrochemical performances.

Ni-rich NMC	NMC Synthesis Route	Modification	Current density	Voltage range (V vs. Li/Li+)	Initial discharge capacity (mAh g ⁻¹)	Cycle no.	Final discharge capacity (mAh g ⁻¹)	Capacity retention	Re
NMC622	Co-precipitation	Pristine	0.5C	3.0–4.55	~180.0	200	117.4	65.2 %	[3]

Ni-rich NMC	NMC Synthesis Route	Modification	Current density	Voltage range (V vs. Li/Li+)	Initial discharge capacity (mAh g ⁻¹)	Cycle no.	Final discharge capacity (mAh g ⁻¹)	Capacity retention	Re
		PVA/ γ -Al ₂ O ₃ coating via sol-gel	0.5C	3.0–4.55	~190.0	200	171.0	90.0 %	
	Solid-state	Pristine	1.0C	3.0–4.5	201.3	50	174.9	91 %	[4]
		Zr-doping	1.0C	3.0–4.5	196.5	50	192.6	98 %	
		ZrO ₂ coating via solid-state	1.0C	3.0–4.5	193.7	50	174.3	90 %	
	Solid state	Pristine	1.0C	3.0–4.5	181.9	100	166.0	91.3 %	[4]
		rGO coating via wet method	1.0C	3.0–4.5	183.4	100	179.9	98.1 %	
NMC811	Co-precipitation	Pristine	1.0C	3.0–4.3	172.0	100	126.6	73.6 %	[4]
		Al-doping	1.0C	3.0–4.3	171.7	100	165.2	96.2 %	
	Co-precipitation	Pristine	0.5C	2.8–4.3	178.0	184	142.4	80 %	[4]
		Fe-doping	0.5C	2.8–4.3	195.0	421	156.0	80 %	
	Co-precipitation	Pristine	0.33C	2.8–4.3	185.0	300	132.5	71.6 %	[3]
		Ni-dual concentration gradient	0.33C	2.8–4.3	188.8	300	167.1	88.5 %	
	Sol-gel	Pristine	0.1C	3.0–4.8	201.8	100	133.2	66.0 %	[3]
		Mg/Zr co-doping	0.1C	3.0–4.8	232.2	100	163.7	70.5 %	
	Hydrothermal	Pristine	1.0C	2.8–4.5	177.7	50	149.3	84.0 %	[4]
		Li ₃ PO ₄ coating via	1.0C	2.8–4.5	206.4	50	191.1	95.6 %	

Ni-rich NMC	Modification	Current density	Voltage range (V vs. Li/Li+)	Initial discharge capacity (mAh g ⁻¹)	Cycle no.	Final discharge capacity (mAh g ⁻¹)	Capacity retention	Re
hydrothermal								

2.1. Co-precipitation

Over the past decades, co-precipitation has garnered significant attention, particularly in Ni-rich cathode materials. This surge in interest can be attributed to its inherent simplicity, controlled over particle morphology, homogenous mixing at the atomic level, and practical scalability, particularly in large industrial scale [10]. This method allows tailoring of both morphology and tap density by tuning of pH, rate of stirring, reaction duration and temperature.

The general procedure for co-precipitation synthesis comprises of two pivotal stages: 1) the controlled creation of an ionic solution to coprecipitate transition metals, and 2) the subsequent sintering of the precursor of these transition metals along with lithium sources [45]. The initial phases of the co-precipitation process necessitate the formulation of an ionic solution containing transition metals in precise molar proportions. Reaction mechanism of co-precipitation is complicated. It requires control of various parameters. Different condition is also required for the addition of Ni, Mn, and Co ion ratio to ensure uniform precipitation in NMC system. Subsequently, a precipitating agent such as a sodium hydroxide solution (NaOH), and a chelating agent like ammonium hydroxide (NH₄OH) solution are introduced. This step is typically conducted within a controlled setting by regulating the solution's pH and inert atmosphere to yield a synthesized precipitate, often referred to as the precursor. The adjustment of these parameters is critical, as it profoundly affects the final product's morphology, particle uniformity, phases, and consequently, its electrochemical behaviour. Following the synthesis, the obtained precursor is rinsed with deionized water to eliminate any impurities and is then subjected to a drying process. This is to ensure that the precursor is free from leftover water and solvents. The dried NMC precursor is then sintered, lithiated and calcined to form α -NaFeO₂.

2.1.1. Synthesis parameter

Three types of co-precipitation methods which are commonly used in the mass production of cathode for Li-ion batteries based on different types of transition metals and Li salts, are the hydroxide co-precipitation method, carbonate co-precipitation method, and oxalates co-precipitation method [46,47]. The hydroxide co-precipitation method is one of the earliest established co-precipitation techniques and remains the preferred choice for crafting nickel manganese cobalt hydroxide, $\text{Ni}_x\text{Mn}_y\text{Co}_{1-x-y}(\text{OH})_2$, followed by carbonate and oxalate co-precipitation [46,47]. The hydroxide co-precipitation method is projected as the most efficient and cost-effective method for producing particles with high tap density and controlled particle size distribution. However, this approach encounters challenges when aiming to create precursors with high manganese content, as Mn^{2+} can readily undergo oxidation to Mn^{3+} during the synthesis process [48]. The co-existence of these Mn impurities with manganese hydroxide resulted in the formation of manganese oxyhydroxide (MnOOH) and caused a deviation from the intended stoichiometry. Zhou et al. [48] reported that the $\text{Ni}_x\text{Mn}_{1-x}\text{O}_2$ hydroxide precursor, prepared in air exhibited a strong diffraction peak at $2\theta = 11.5^\circ$, which indicated the presence of a layered double hydroxide (LDH). Presence of LDH can be attributed to the large spacing between $\text{M}(\text{OH})_2$ slabs, which occurs from the incorporation of Mn^{3+} into the materials during synthesis. Hydroxide primary particles also tend to adopt lamellar or needle-like morphology, which poses a challenge in preparing densely packed secondary particles [10].

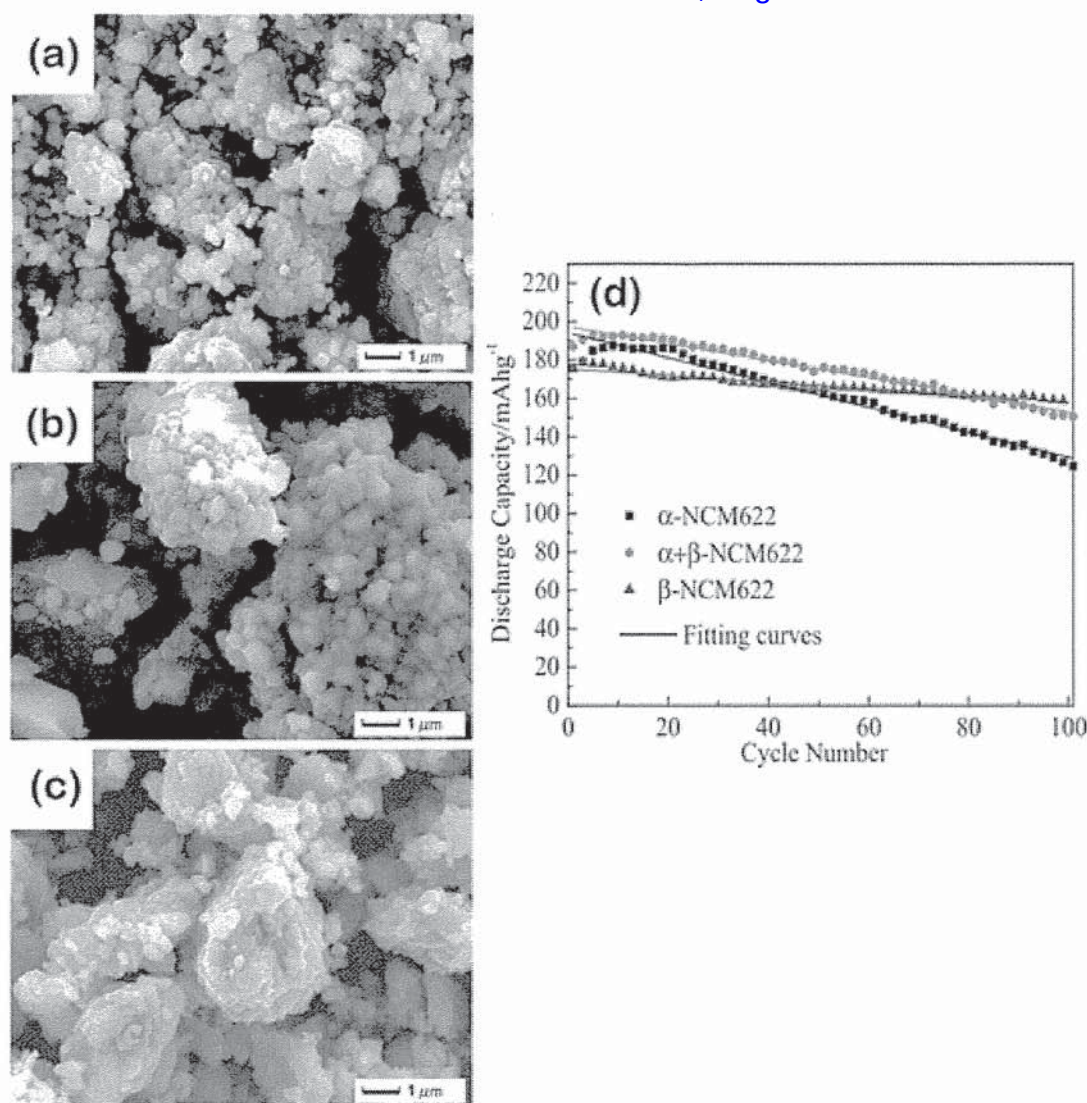
Reaction time, pH and temperature of the ionic solution are important factors that influence particle morphology and electrochemical characteristics of synthesized NMC material, especially via the hydroxide co-precipitation method [10]. A study conducted by Cheralathan et al. shows that longer reaction time leads to a more spherical particle and a larger tap density. The $\text{Ni}_{0.80}\text{Co}_{0.15}\text{Mn}_{0.05}(\text{OH})_2$ precursors prepared at different precipitation times of 1, 8, 24, and 32h show an agglomeration of irregular-shaped fine particles formed during the early hour of mixing. Upon 24h of reaction time, the particles grow gradually and develop a smoother and more uniform spherical morphology without further agglomeration. After 32h of precipitation, a steady state is reached where precipitation has a clear spherical shape and narrow size distribution.

Degree of transition metal precipitation is controlled by pH value, which is determined by the ratio of ammonia to sodium hydroxide. It has been reported that the pH can control the nucleation growth, morphology, shape, and particle size distribution and thus affect the tap density of synthesized NMC material [10,47,49]. For instance, Vu and Lee [49] reported an increase in tap density for $\text{NMC811}(\text{OH})_2$ from 1.91 to 1.26gcm^{-3} when increasing pH from 11.5 to 11.8. Liang and co-workers synthesized $\text{NMC622}(\text{OH})_2$ at various pH values by co-precipitation. At a lower pH of 11.2, spherical and uniform $\text{NMC622}(\text{OH})_2$ has the highest

Case 2:24-cv-10546-BRM-KGA ECF No. 30-48, PageID.4731 Filed 11/25/24 Page 15 of 69

tap density of 1.65 gcm^{-3} in comparison with pH values of 11.5 (1.47 gcm^{-3}) and 11.8 (1.05 gcm^{-3}).

During co-precipitation, the formation of NMC is governed by the reaction temperature. Precipitation of $\text{Ni}_x\text{Mn}_y\text{Co}_{1-x-y}(\text{OH})_2$ precursor and the nickel hydroxide ($\text{Ni}(\text{OH})_2$) possess similar crystal layered structures. There are 2 major phases of $\text{Ni}(\text{OH})_2$ i.e. the α - $\text{Ni}(\text{OH})_2$ and the β - $\text{Ni}(\text{OH})_2$. At low synthesis temperature ($20\text{--}50^\circ\text{C}$), the precipitation of $\text{Ni}_x\text{Mn}_y\text{Co}_{1-x-y}(\text{OH})_2$ precursor favours α - $\text{Ni}(\text{OH})_2$. On the other hand, at elevated temperature, the precipitation tends to follow the more crystalline β - $\text{Ni}(\text{OH})_2$ [50,51]. However, as the precursor material, the amorphous and unstable α - $\text{Ni}(\text{OH})_2$ is not favourable. Xu et al. [51] have reported on the effect of α , β , and the intermediate $\alpha+\beta$ phases of precursors on the formation of $\text{LiNi}_{0.6}\text{Mn}_{0.2}\text{Co}_{0.2}\text{O}_2$ (NMC622). The NMC622, synthesized from β -phase (β -NMC622) exhibits an excellent hexagonal and layered structure. It shows the highest c/a than the NMC622 synthesized from α -phase (α -NMC622) and $\alpha+\beta$ -phase ($\alpha+\beta$ -NMC622). Fig. 3(a) and (b), and 3(c) display the morphologies of α -NMC622, $\alpha+\beta$ -NMC622, and β -NMC622, respectively. The authors reported that the smooth, quasi-spherical and good crystallization of β -NMC622 is attributed to the β -phase in NMC622 (cf. Fig. 3(b) and (c)). The β -phase precursor exhibits a more orderly matrix structure than α -phase. In addition, the β -NMC622 exhibits a better cycle stability as compared with α -NMC622 and $\alpha+\beta$ -NMC622, as shown in Fig. 3(d). It maintains 91.7% of its capacity after 100 cycles.



Download : Download high-res image (775KB)

Download : Download full-size image

Fig. 3. SEM images of NMC622 samples α -NMC622 (a), $\alpha+\beta$ -NMC622 and (b), β -NMC622 (c), and (d) the cycle performance of prepared NMC 622. Reprinted with permission from Ref. [51], Copyright 2018 Elsevier.

High synthesis temperature has been reported in increasing the particle size and tap density of precursors [48,52]. Zhou et al. [48] reported the effect of temperature on a series of $\text{Ni}_x\text{Mn}_{1-x}(\text{OH})_2$ mixed hydroxide with $x=1, 5/6, 2/3, 1/2$ and $1/3$. The samples were prepared by four different co-precipitation routes and were characterized by XRD, chemical analysis, and SEM techniques. They reported that dense and spherical hydroxide $\text{Ni}_x\text{Mn}_{1-x}(\text{OH})_2$ with a mean size of $10\mu\text{m}$ can be produced with the most controlled condition of pH and a reaction temperature of 60°C . On the other hand, Zhang and co-workers [52] prepared the NMC111 at 60°C by carbonate co-precipitation method. The resultant NMC111 forms dense spherical particles with the good sphericity and particle integrity. The NMC111 precursor

maintains a single-phase layered structure and lower cation mixing for co-precipitation temperature below 60°C. Above 60°C, the Mn_3O_4 and MnO_2 impurities are produced. The impurities affect the spherical and decrease the integrity of the particle. Dense spherical particle is beneficial to its electrochemical performance. Higher energy facilitates the formation of dense spherical particle. For example, material synthesized at 60°C shows higher initial discharge capacity of about 162.5 mAhg^{-1} and good capacity retention over 100 cycles. As a result, reaction temperatures of 50–60°C were widely used to produce the NMC precursors [[52], [53], [54], [55]]. On the other hand, amorphous and unstable $\alpha\text{-Ni(OH)}_2$ crystal structure as well as low tap density are the outcomes of low reaction temperature. In addition, the adverse effect of excess reaction temperature is the formation of large primary particle size and impurities such as Mn_3O_4 and MnO_2 .

Another factor that governs the morphology and electrochemical performance of NMC is thermal treatment process. High temperature thermal treatment of the precipitate is known to result in better crystallinity. However, it comes with unfavourable higher cation mixing and larger particle size, which leads to lower surface area. Zheng et al. [55] revealed that the $\text{LiNi}_{0.76}\text{Mn}_{0.14}\text{Co}_{0.1}\text{O}_2$ synthesized at higher calcination temperature ($\geq 800^\circ\text{C}$) shows inferior long-term cycling stability and rate capability. The $\text{LiNi}_{0.76}\text{Mn}_{0.14}\text{Co}_{0.1}\text{O}_2$ possess large primary particles ($>1 \mu\text{m}$), which causes severe formation of micro-strain and crack upon the lithium-ion de-intercalation process. Vu and Lee [49] prepared NMC811 with mixed hydroxide salt. The samples are annealed at 780°C, 800°C and 820°C for 16h. XRD results revealed that NMC811 synthesized at 780 and 800°C have better ordered layered structure with lower $\text{Li}^+/\text{Ni}^{2+}$ cation mixing. When discharged at 3.0–4.3V, as compared to others, the NMC811 calcined at 800°C possessed higher initial discharge capacity of 193.7 mAhg^{-1} at a current density of 18.5 mAhg^{-1} with a good rate capability. Temperatures from 750 to 800°C are the optimum temperature for the heat treatment process of Ni-rich NMC [49,55,56]. Poor crystal layered structure and inadequate phase transformation are the result of low calcination temperature. On the other hand, excess calcination temperature leads to high Li loss and large particle size.

It is widely recognized that NH_4^+ ion plays an important role in preventing the emergence of undesired phases and promoting the formation of dense sphere-like hydroxide. During the production process of the $\text{Ni}_x\text{Mn}_y\text{Co}_{1-x-y}(\text{OH})_2$ precursor, a combination of Ni(OH)_2 , Co(OH)_2 , and Mn(OH)_2 phases can commonly exist due to differences in solubility. If the chelating agent NH_4OH is not utilized during the synthesis process, there is a possibility for these mixed phases to form impurities in the end product [48]. Thus, it is important to incorporate a suitable concentration of NH_4OH to form a single-phase and well-homogeneous $\text{Ni}_x\text{Mn}_y\text{Co}_{1-x-y}(\text{OH})_2$ precursor. The role of NH_3 concentration on NMC

Case 2:24-cv-10546-BRM-KGA ECF No. 30-48, PageID.4734 Filed 11/25/24 Page 18 of 69

particle morphology and size has been investigated by many researchers. Several studies suggest that with increasing NH_3 concentration, the tap density increases, and the secondary spherical particles become more uniform with narrower particle size distribution [48,49,57].

Zhu et al. [57] studied the effect of NH_3 concentration on NMC811 precursor tap density and electrochemical performances. It can be observed that as the NH_3 concentration increases to 1 molL^{-1} , the tap density increases to 1.95 gcm^{-3} and decreases simultaneously thereafter. NMC811 at a concentration of 0.97 molL^{-1} demonstrates the highest RIR value of 1.78, indicating reduced cation mixing in the material. This material achieves the highest initial discharge capacity of 200.1 mAhg^{-1} and exhibits a Coulombic efficiency of 89.16%. Another study by Duan et al. [58] also shows that NMC811 with an optimised molar concentration of 0.55 molL^{-1} and pH 11.4 has the densest and firmest structure with the highest tap density of 2.115 gcm^{-3} . The material produced a well-ordered layered crystal structure with a discharge capacity of 189.4 mAhg^{-1} and capacity retention of 96.3% after 200th cycles at 1C rate.

The types of impeller blades either radial, axial, or both, have a direct influence on the manner and orientation of mixing NMC precursor. It is ultimately shaping the particle uniformity and influences the tap density and particle size distribution of NMC cathode precursors. A recent study by Alpay and Kelles [54] shows how the impeller type affects the flow pattern, and consequently, the final electrochemical performance of NMC811 using both simulation and experimental. NMC811 synthesized using a propeller-type impeller delivered a 174.58 mAhg^{-1} discharge capacity and 96.02 % Coulombic efficiency. On the other hand, at the same C/20 rate, the NMC811 synthesized by the Rushton turbine yielded a 100.12 mAhg^{-1} discharge capacity. This proves that the impeller geometry affects strongly the flow pattern and hence the cathode performance. Zhu et al. [53] examined the effect of axial and radial flow on NMC622 precursor. The propeller turbine at 1100rpm results in 2.0 gcm^{-3} tap density of NMC622(OH)_2 precursor. Upon calcination, the tap density increased to 2.5 gcm^{-3} with the average particle size of $12 \mu\text{m}$, which remained unchanged upon sintering. The resulting NMC622 cells showed an initial discharge capacity of 177.6 mAhg^{-1} at 2.7–4.3V and 0.2C. After 200 cycles at 2C, it retained 97.9% of its capacity. A 10–15% decrease in capacity and capacity retention can be observed with impeller blades such as the flat-blade and Rushton turbines.

Another vital consideration is the stirring rate which governs the shear rate within the system and thereby influences particle growth. Increasing the stirring rate results in a higher frequency of particle collisions and interactions with the walls of the precipitation

reactor. This acceleration promotes the formation of uniformly spherical particles and contributes to improve tap density of the material and thus, improve the electrochemical behaviour. Vu and Lee [49] examined the effect of stirring at the rate speed of 500, 600, and 800rpm on the particle morphology of NMC811. It is found that the particle NMC811 becomes larger with approximately $20\mu\text{m}$ at a lower stirring rate (500rpm) compared to 800rpm ($13\mu\text{m}$). Dong et al. studied the effect of different stirring rates of 600, 800, 1000, and 1200rpm on the co- $\text{Ni}_{0.6}\text{Mn}_{0.2}\text{Co}_{0.2}(\text{OH})_2$ precursor. It can be observed that the particles agglomerated irregularly at a low stirring rate of 600rpm. As the stirring rate was increased to 1000rpm, the spherical particles were densely packed with a smoother surface. Further observation at 1200rpm shows that some particles were cracked or deformed at this stage which indicates that the tolerance level has exceeded and deformed the NMC622 particle.

2.1.2. Modification via Co-precipitation

The purpose of using Ni-rich NMC as cathode battery material is to replace the cobalt content with Nickel to further reduce the cost and improve battery capacity. However, the Ni-rich NMC suffers from stability issues. Dopants and surface coatings are popular solutions to these problems.

2.1.2.1. Doping

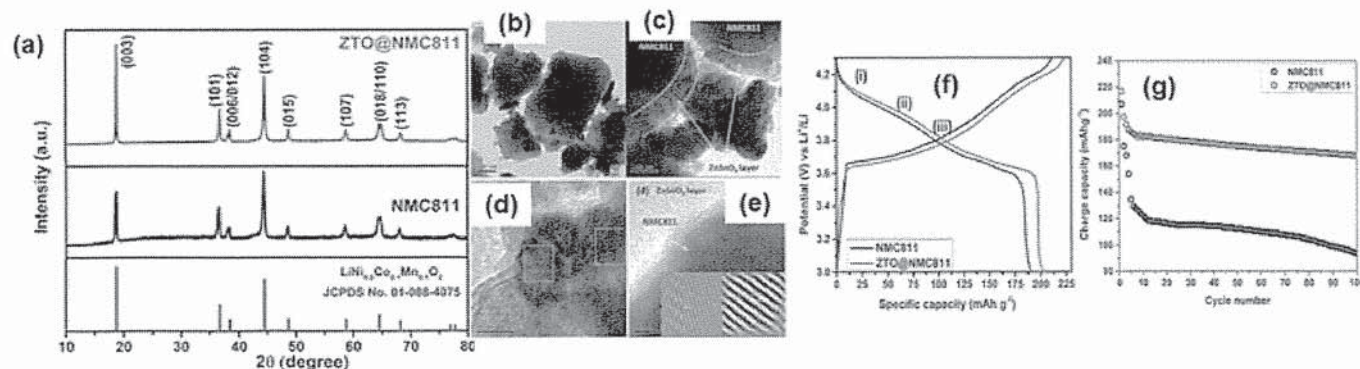
The incorporation of dopants has been reported to strengthen the transition metal (TM)-oxygen bonds and consequently, reduce oxygen release in the material. This is one of the ways to limit the NMC degradation upon higher cycling. Metal dopants such as Fe [43], Ti [59], Al [60], Mg [61], Y [62] and etc can reduce $\text{Li}^+/\text{Ni}^{2+}$ mixing and provide charge compensation that balances the electrostatic repulsion between oxygen atoms.

A study conducted by Zha et al. [43] revealed that by partially replacing Co with Fe to form a layered structure, the electrochemical performance of the LIB with much better cycling stability and higher capacity can be achieved. The $\text{LiNi}_{0.8}\text{Co}_{0.07}\text{Fe}_{0.03}\text{Mn}_{0.1}\text{O}_2$ (Fe3-NCM871) was synthesized via the co-precipitation method followed by the sintering process. The obtained XRD spectra can be indexed to a hexagonal $\alpha\text{-NaFeO}_2$ layered structure and space group R-3m. The noticeable splits of (110)/(018) peaks in both samples indicated well-developed layered structures. Left-shift of the (003) and (104) peaks of Fe3-NCM871 indicated the enlargement of these lattices. Fe3-NCM871 sample possessed a high $I(003)/I(104)$ ratio value which this value reflects a low degree of $\text{Ni}^{2+}/\text{Li}^+$ cation mixing and this result was further supported by the computational study. The pristine and Fe3-NCM871 cathodes produced first discharge capacity of 188.7, and 207.5 mAh g^{-1} at 0.1C. Fe3-NCM871

maintained a good cycle stability performance with an 80 % state of health after 400 cycles. The high capacity of Fe₃-NCM871 was attributed to the reduction of Ni/Li mixing, which increased the diffusion rate of Li⁺. On the other hand, the high cycle stability was due to the elimination of the harmful effect of H₂→H₃ lattice distortion, which was confirmed by Ex-situ XRD analysis.

2.1.2.2. Coating

Sanad et al. [63] synthesized NMC811 and a new perovskite-type ZnSnO₃ (ZTO) film later coated on the surface of NMC811 via in-situ co-precipitation method at low annealing temperature. XRD data shows that the diffraction peaks confirmed the formation of a single phase of rhombohedral structure (R-3m space group), of hexagonal NMC811 structure which well matched with JCPDS 1-88-4075. The XRD pattern of the rhombohedral phase (JCPDS 28-1486) of pure distorted perovskite ZnSnO₃ also matched with the coated ZTO-NMC811 sample as displayed in Fig. 4(a). It revealed that RIR value of ZTO-NMC811 is higher than that of NMC811, indicating that lower cation mixing occurred in the material. Generally, both NMC811 and ZTO-NMC811 showed rhombohedral-like morphology with 1.5–2.5 μm dimensions. Furthermore, from the TEM and HRTEM inspections, 1 wt% ZTO@NMC811 is covered with a layer of agglomerated spheres of ZnSnO₃. The thickness of the layer is close to 100 nm, as seen in Fig. 4 (b) and (c). The ZTO@NMC811 has two lattice fringes i.e. 0.39 nm and 0.46 nm. The 0.39 nm is corresponding to the (110) and (003) lattice planes of R-3c, while the 0.46 nm is attributed to the R-3m space groups fringes (cf. Fig. 4(d) and (e)). The ZTO-NMC811 delivered a charge capacity of 223 mAhg⁻¹ and a discharge capacity of 202 mAhg⁻¹ after the first cycle (Fig. 4 (f)). At 0.1C, the surface-modified NMC811 maintained about 73 % of its initial capacity from 25th to 35th cycle, as shown in Fig. 4 (g). This suggests that the ZTO coating acts as a heat-resisting interface, which improves the thermal stability of pristine NMC811 and hence its performance.



Download : Download high-res image (489KB)

Download : Download full-size image

Case 2:24-cv-10546-BRM-KGA ECF No. 30-48, PageID.4737 Filed 11/25/24 Page 21 of 69

Fig. 4. (a) XRD patterns of pristine NMC 811 and ZTO@NMC811, HRTEM images of (b), (c) lattice fringes, (d), (e) SAED pattern of ZTO@NMC811, (f) Charge-discharge profile of the first cycle at 0.1C, and (g) Cyclic performance of NMC 811 and ZTO@NMC811. Reprinted with permission from Ref. [63], Copyright 2023 Elsevier.

2.2. Sol-gel

Sol-gel is a versatile synthesis method for producing solid materials, starting from solution through a transformation from liquid precursors to a colloidal solution (sol) and finally to an integrated network structure (gel) [64,65]. Initially, a precursor solution is prepared, which typically consists of metal alkoxides dissolved in a solvent. Then hydrolysis reaction occurs, where the metal alkoxides react with water molecules to form metal hydroxides or metal oxide precipitates. This reaction can be catalysed by acids or bases, depending on the desired properties of the resultant material [66,67]. As the hydrolysis reaction progresses, the sol undergoes a transformation from a homogeneous solution to a colloidal suspension containing nano-solid particles dispersed in a liquid medium. Once hydrolysis has occurred, the hydroxyl groups on the nanoparticles undergo condensation reactions which involve the reaction of two hydroxyl groups, resulting in the elimination of a water molecule and the formation of a covalent bond between the nanoparticles. This process leads to the formation of a three-dimensional network or gel structure. Subsequently, the gel undergoes drying or aging process, where the liquid component is gradually removed through evaporation. This drying step further consolidates the gel structure and removes the remaining solvent, resulting in the formation of a solid material [65,68].

The sol-gel process has several advantages, including the ability to synthesize materials with outstanding purity and homogeneity at low synthesis temperatures. This approach also offers structure and morphology manipulation by altering the pH [66], temperature [69,70], and drying conditions [71,72] as well as by utilizing various types of solvents [73,74] and chelating agents [75]. Catalysts, typically acid or base catalysts, can be added to speed up the hydrolysis and condensation reactions that transform the sol into a network of gel-like molecules [76].

2.2.1. Effect of synthesis parameter

Synthesis parameters can greatly affect material properties and accordingly the electrochemical performances. The growth of the synthesis cathode material is significantly influenced by the pH, temperature, types of solvents, chelating agents, presence of catalyst, and drying conditions. However, most of these parameters are rarely studied in the

Case 2:24-cv-10546-BRM-KGA ECF No. 30-48, PageID.4738 Filed 11/25/24 Page 22 of 69

synthesis of cathode materials, especially in Ni-rich NMC. Only few research works on the effect of chelating agents and drying parameters on the synthesis of NMC-based cathode materials have been reported.

Kızıltas, -Yavuz et al. [77] used table sugar as a chelating agent to prepare NMC 111. The XRD peaks obtained from the synthesized sample can be well-indexed to a hexagonal lattice of a-NaFeO₂-type layered structure with space group R-3m without any impurity. The sample had a quasi-spherical form with a diameter distribution of 300–500nm with a first discharge capacity of 149 mAh g⁻¹ at 0.1C. Singh et al. [78] studied the effect of citric acid content on the production of NMC 111. In their study, the concentration of citric acid employed as a chelating agent has no effect on the material structure or electrical conductivity. However, it does influence particle size and metal stoichiometry composition.

Li et al. [75] studied the effect of three different chelating agents which are citric acid (C-622), glucose (G-622), and sucrose (S-622) on the production of NMC 622 from waste nickel–cobalt–manganese ternary cathode materials. SEM analysis shows that there is no difference in morphology between the samples, as all of them consist of spherical particles. However, different chelating agents play a role in crystal growth, with S-622 producing the largest particles among the samples. The G-622 sample demonstrated the highest electrochemical performance, exhibiting an initial discharge capacity of 176.9 mAhg⁻¹ and retaining 95.8% of its initial capacity after 50 cycles at 0.2C. This exceptional performance can be attributed to G-622's minimal cation mixing, low impedance, and excellent reversibility of the redox reaction.

Overall, in the sol-gel process, a stoichiometric amount of lithium salt is commonly mixed together with other inorganic metal salt or metal alkoxide precursors with the chelating agent in distilled water. The effect of the chelating agent is the most studied parameter in sol-gel synthesis for cathode battery applications as it plays a significant role in controlling the hydrolysis and condensation reactions. Citric acid is the commonly used chelating agent due to its low-cost and having many functional groups of –OH and –COOH that possess strong chelating ability [79]. Glucose [75], sucrose [75], urea [80], ethylene diamine tetra-acetic acid (EDTA) [79], and glycolic acid [81] are other options as chelating agents. Subsequently, ammonia solution is generally added as a catalyst and a pH regulator in the synthesis. In LIBs, the cathode materials are usually synthesized via sol-gel in a basic environment to promote hydrolysis and condensation of the precursor molecules. By varying the ammonia concentration, it is also possible to control the growth and aggregation of particles, resulting in particles of different sizes and shapes [82,83]. The resultant gel formation is usually dried at a temperature above the boiling point of water

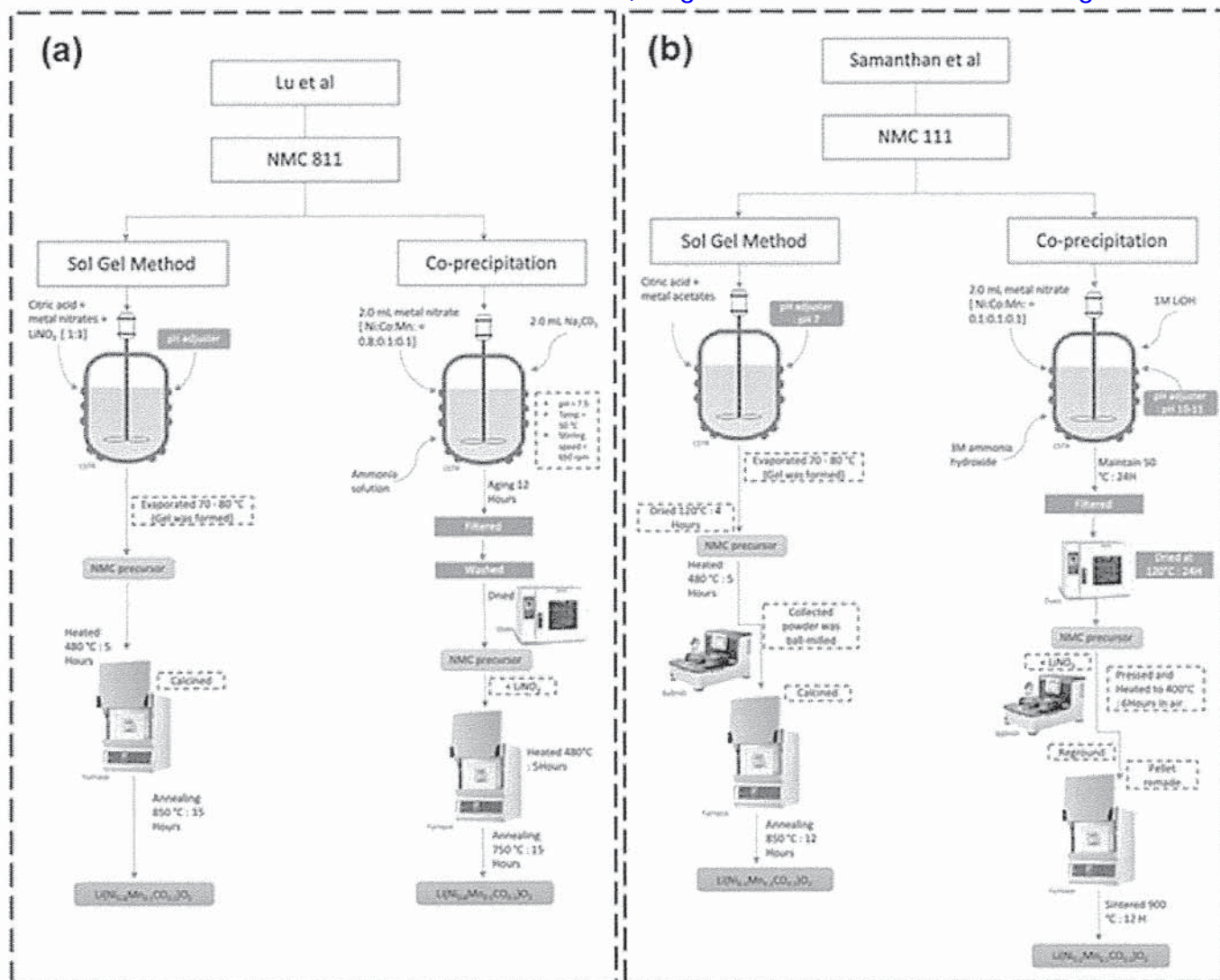
Case 2:24-cv-10546-BRM-KGA ECF No. 30-48, PageID.4739 Filed 11/25/24 Page 23 of 69
(120–160°C). Both drying temperature and duration have been reported to affect the layered structure of the obtained cathode materials. Then, the obtained solid powder is further sintered to remove impurities and organic compounds. The synthesis of Ni-rich NMC via sol-gel has been the subject of multiple published research [[84], [85], [86]].

However, this synthesis technique comes with few disadvantages such as long processing time due to solvent evaporation, gel formation, and subsequent drying or curing steps. The sol-gel technique entails multiple stages and requires careful regulation of various parameters, including temperature, pH, precursor concentration, ageing, and drying condition. This complexity can make it difficult to optimize and reproduce the process consistently which might lead to higher production costs. Besides, the synthesized materials may experience shrinkage during the gelation and drying phases, which may result in cracking or deformation. Therefore, scaling the procedure up to industrial levels can be difficult due to critical factors such as consistency, repeatability, and production cost.

2.2.2. Comparison between sol-gel and co-precipitation synthesis methods

Sol-gel and co-precipitation are both widely used methods for the preparation of cathode batteries. They are often compared because they share some similarities: 1) They both involve the formation of materials from a liquid solution. The raw materials are dissolved in a solvent, and the desired material is then formed through chemical reactions and precipitation. 2) Both are versatile methods to obtain nanoparticles with desired properties by manipulating reaction parameters such as temperature, pH, solvent, and precursor. This makes both methods attractive for applications that require precise control over particle properties like electrochemical energy storage devices.

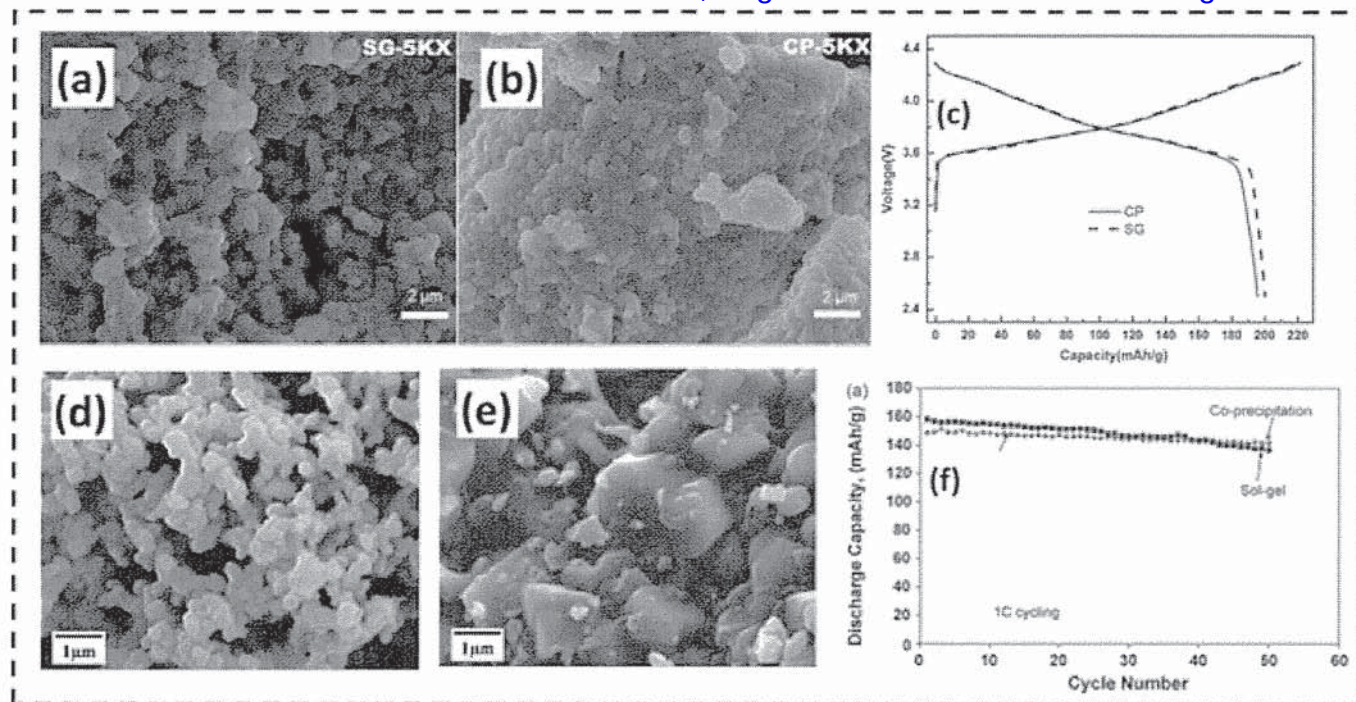
A comparison study of different synthesis methods of NMC 811 via sol-gel and co-precipitation was conducted by Lu et al. [87]. The flow of both synthesis processes is illustrated in Fig. 5(a). The XRD patterns of NMC 811 from both synthesized techniques displayed well-crystallized layered structures with space group R-3m. However, from the refinements, the NMC 811 from sol-gel possessed lower $\text{Li}^+/\text{Ni}^{2+}$ cations mixing compared to the co-precipitation method. The NMC 811 synthesized via sol-gel also exhibited a more porous structure and less aggregation (cf. Fig. 6(a) and (b)), which provided higher surface area and better electrode/electrolyte contact. Due to these characteristics, the NMC 811 synthesized via sol-gel displayed an initial discharged capacity of 200.1 mAhg^{-1} at 0.1 C with 89.1 % capacity retention after 50 cycles which is slightly better than co-precipitation method with $195.7 \text{ mAh}\cdot\text{g}^{-1}$ at 0.1 C with 85.2 % capacity retention, respectively (cf. Fig. 6(c)).



Download : Download high-res image (808KB)

Download : Download full-size image

Fig. 5. Illustration of the comparison synthesis process of (a) NMC 811 by Lu et al. and (b) NMC 111 by Samanthan et al.



Download : Download high-res image (748KB)

Download : Download full-size image

Fig. 6. FESEM images of the NMC 811 powders synthesized via (a) sol-gel and (b) co-precipitation, (c) the initial charge and discharge curves of NMC 811 synthesized via sol-gel (SG) and co-precipitation (CP). Reprinted with permission from Ref. [87], Copyright 2013 Elsevier. SEM images of the NMC 811 powders synthesized via (d) sol-gel and (e) co-precipitation. (f) rate cycling performance of NMC 111 electrode prepared by sol-gel, and co-precipitation methods at 1C. Reprinted with permission from Ref. [88], Copyright 2010 Elsevier.

Another comparison study of different synthesis methods of NMC 111 via sol-gel and co-precipitation was conducted by Santhanam et al. [88]. The flow of both synthesis processes is in Fig. 5(b). The XRD patterns of NMC 111 can be indexed to the hexagonal lattice of a- NaFeO_2 -type. Splitting peaks at (006)/(102) and (108)/(110) were distinctly observed which demonstrated the formation of well-ordered layered structures. Both samples possessed an $I(003)/I(104)$ ratio value of around 1.3 of which this value reflects a low degree of $\text{Ni}^{2+}/\text{Li}^+$ cation mixing. NMC 111 prepared by the co-precipitation method shows the formation of larger particles (1–2 μm) in contrast to those prepared using the sol-gel method (0.3–0.4 μm) (cf. Fig. 6(d) and (e)). NMC 111 synthesized via sol-gel and co-precipitation delivered 168 and 158 mAh g^{-1} , respectively at 0.1C. It also displayed higher discharge capacity than co-precipitation at all current densities from 0.1 to 8.0C. However, for cycling performances, the NMC 111 synthesized via co-precipitation with a capacity retention ratio of about 95%

when compared to that of sol-gel is only 87% at 1.0C (cf. Fig. 6(f)). The authors stated that the smaller particle size of NMC 111 synthesized by sol-gel contributes to its high discharge capacity and rate capability. This is because small particles provide short diffusion lengths for lithium-ion transport within the particles and therefore increase the insertion and de-insertion of lithium ions. Since the small particles have a high surface area, they have high tendency to exhibit side reactions with the electrolyte that will lead to poor performance when long-cycling.

In summary, sol-gel synthesis and co-precipitation are compared due to their shared solution-based nature and the versatility in obtaining desired particle properties. However, sol-gel synthesis offers more process control, higher purity, and better homogeneity, while co-precipitation is often more cost-effective and suitable for large-scale production. The choice between these methods depends on the specific requirements of the desired material.

2.2.3. Modification via sol-gel

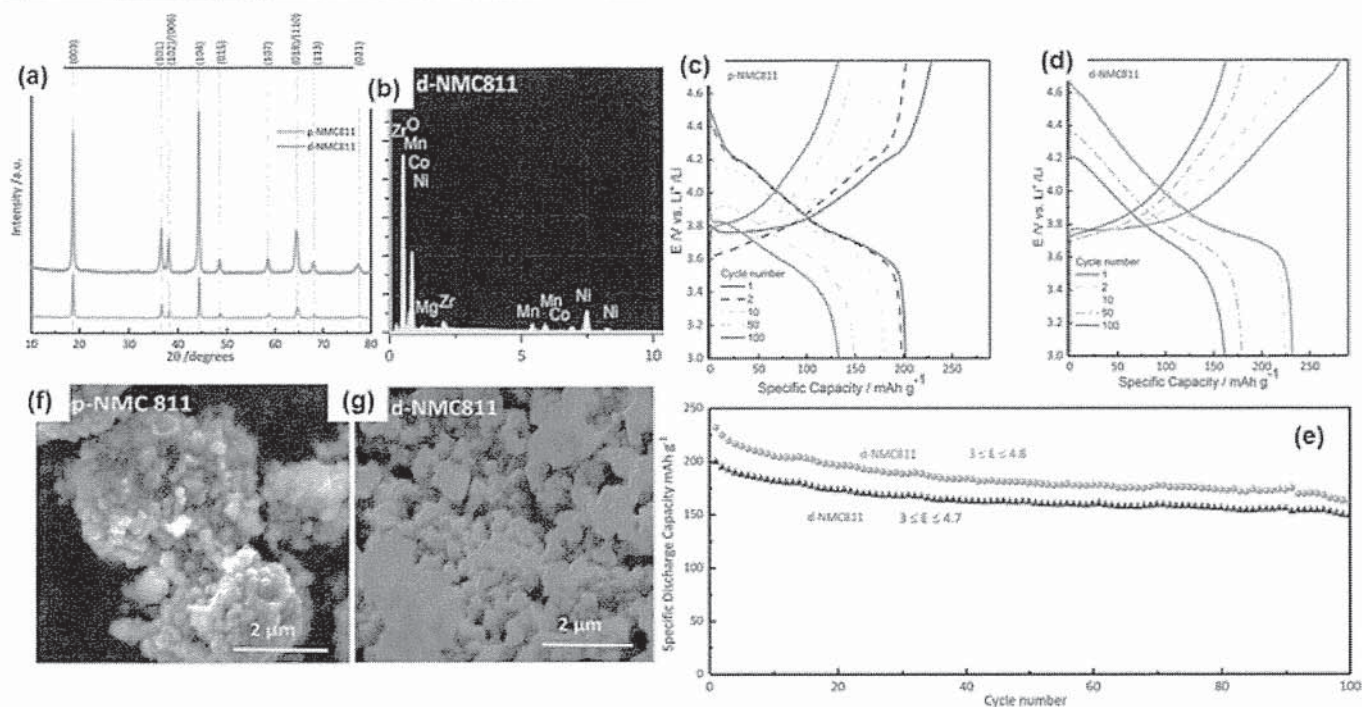
2.2.3.1. Doping

Doping refers to the intentional introduction of small amounts of specific elements or impurities into the crystal structure of the material. Doping is commonly employed to modify the electrochemical properties of NMC and enhance its performance as a cathode material in LIB. In sol-gel synthesis, the doping salts were introduced together with other metal alkoxide precursors.

Darjazi et al. [32] improved the electrochemical performance of NMC811 by Mg and Zr co-doping via an acid-assisted sol-gel method ($\text{LiNi}_{0.8}\text{Co}_{0.09}\text{Mn}_{0.1}\text{Mg}_{0.05}\text{Zr}_{0.05}\text{O}_2$). The pristine and co-doped NMC811 were labelled as *p*-NMC811 and *d*-NMC811, respectively. Fig. 7(a) shows the XRD patterns of both samples and they displayed well-crystallized layered structures with space group R-3m. Evidence from XRD refinement via the Rietveld method suggested that the interlayer spacing increased with doping elements. This is due to the large ionic radius of Zr^{4+} (0.79Å) and Mg^{2+} (0.72Å), and therefore expanded the Li-ion pathways. The XPS and EDX studies confirmed the correct stoichiometry ratio of both samples and the presence of Zr and Mg elements in *d*-NMC811 (cf. Fig. 7(b)). The morphology and structure of *d*-NMC 811 displayed a much smaller particle size with a more uniform particle distribution when compared with *p*-NMC811 (cf. Fig. 7(f) and (g)). At 0.1C, the *p*-NMC811 delivered a discharge capacity of 201.8 mAh g⁻¹ and *d*-NMC811 delivered a discharge capacity of 232.2 mAh g⁻¹. After 100 cycles, the *p*-NMC811 and *d*-NMC811 maintained 66.0 and 70.5 % of their initial capacity, respectively (cf. Fig. 7(c)–(e)). The

Case 2:24-cv-10546-BRM-KGA ECF No. 30-48, PageID.4743 Filed 11/25/24 Page 27 of 69

improved performance of the LIB can be attributed to the improved structural and morphological properties of Mg and Zr co-doped NMC 811.



Download : Download high-res image (793KB)

Download : Download full-size image

Fig. 7. (a) XRD patterns of *p*-NMC811 and *d*-NMC811, (b) EDX spectrum of *d*-NMC811, charge-discharge profile at different cycle numbers of (c) *p*-NMC811, and (d) *d*-NMC811, (e) cycle performance, SEM images of (f) *p*-NMC811, and (g) *d*-NMC811. Reprinted with permission from Ref. [32], Copyright 2022 Elsevier.

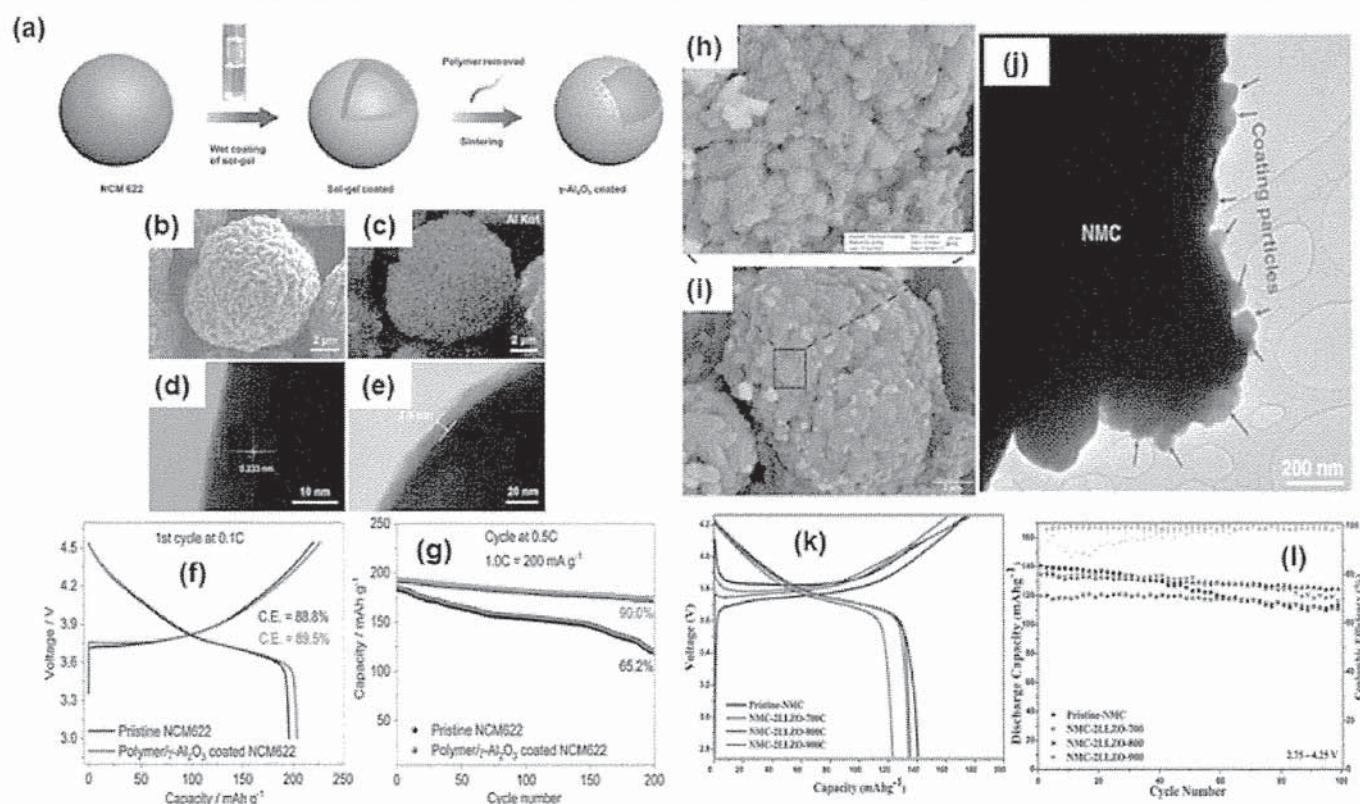
2.2.3.2. Coating

Coatings are commonly used to improve the performance, stability, and safety of NMC cathodes by applying a thin layer of material or film onto the surface of NMC particles. The coating technique on the NMC materials can be done via the sol-gel method. The usual approach for preparing the coating is first to dissolve the precursor of the coating material in an aqueous-based solution. Next, the NMC cathode materials are dispersed into the solution under continuous stirring and heating. Then, the chelating agent is gradually added into the solution. The solution is kept under stirring and heating until the solvent is dried. Then, the solid sample is collected for annealing process.

Wu et al. [39], used a polymer-aided sol-gel process to develop a thin coating consisting of a microporous γ - Al_2O_3 protection layer on the NMC cathodes as illustrated in Fig. 8(a). The

Case 2:24-cv-10546-BRM-KGA ECF No. 30-48, PageID.4744 Filed 11/25/24 Page 28 of 69

polyvinyl alcohol (PVA) polymer was used as a template to facilitate the film forming while leaving micropores in the film after sintering. The PVA/ γ - Al_2O_3 sol-gel was first prepared before being mixed with NCM622 particles for 30 min under continuous stirring. This coating process was performed by sintering at 550°C for 5 h to remove the polymer while leaving the γ - Al_2O_3 coating layer. Both samples exhibited a typical a- NaFeO_2 -type layered structure with no visible XRD peak of the Al_2O_3 coating layer; this is due to the ultrathin thickness of the coating layer. Further analysis by XRD refinement suggested that this coating did not change the internal structural details. The coating was homogenous and thin with a thickness of $\sim 7.8\text{ nm}$ as displayed by EDX (cf. Fig. 8(b) and (c)) and HRTEM images (cf. Fig. 8(d) and (e)). The polymer/ γ - Al_2O_3 -coated NMC 622 delivered 203.97 mAhg^{-1} capacity compared to the pristine with 196.07 mAhg^{-1} as displayed in Fig. 8(f). Fig. 8(g) shows the coated sample retained 90% of its capacity at 0.5 C after 200 cycles, which was 24.8% higher than that of the pristine sample. The high cycling stability from coated NMC was due to the coating suppressing the dissolution of transition metals.



Download : Download high-res image (990KB)

Download : Download full-size image

Fig. 8. (a) Illustration of PVA/ γ - Al_2O_3 coating process, (b) SEM image, (c) EDX mapping of aluminium, (f) TEM images of (d) pristine NMC 622, (e) PVA/ γ - Al_2O_3 coated NMC 622, (f) first cycle capacity at 0.1 C , and (g) cycling performance at 0.5 C [39]. (h), (i) SEM images, and

Case 2:24-cv-10546-BRM-KGA ECF No. 30-48, PageID.4745 Filed 11/25/24 Page 29 of 69
(j) TEM image of NMC- 2LLZO800, (k) first cycle capacity, and (l) cycling performance at 0.1 C. Reprinted with permission from Ref. [89], Copyright 2023 Elsevier.

Engün et al. [89] used Li ion conductor $\text{Li}_7\text{La}_3\text{Zr}_2\text{O}_{12}$ (LLZO) as a potential coating material for NMC. They studied the performance of the coating by varying the amount of coating (2–12 %) and the annealing temperature (700–900°C). The ZnNO_3 was used as Zn doping source and phase stabilizer in LLZO material synthesis. The NMC powder was mixed with the prepared LLZO solution under continuous stirring for 2 h, with a certain amount of ethylene glycol as a chelating agent. The mixture was dried at 120°C and gel was obtained. The solid sample was collected after subsequent drying processes. All samples exhibited a typical NaFeO_2 -type layered structure. The presence of XRD peaks from LLZO coating is only visible at 12 % amount. The peaks can be indexed to LaMO_3 (M: Ni, Mn, and Co). The formation of LaMO_3 occurred because of the diffusion of lithium from highly concentrated LLZO to NMC. XRD refinement revealed that raising the annealing temperature resulted in an increase in lattice volume due to the diffusion of La and Zr ions from LLZO into the NMC structure. Fig. 8(h) and (i) show SEM images of white island formation on cathode materials, whereas Fig. 8(j) displays the TEM image of the coating particle on the surface of NMC material. STEM-EDX analysis was used to analyse the chemical distribution of the particles. La is strongly diffused inside the cathode materials, Zr remained at the top coating layer and formed ZrO_2 . The Ni, Mn, and Co atoms from NMC cathode were found to diffuse out onto the coating surface. The 2% LLZO with the 800°C annealing temperature (NMC- 2LLZO800) exhibited the best electrochemical performance. Pristine NMC cathode provided a discharge capacity of 141 mAh g^{-1} and capacity retention of 78 %, whereas NMC- 2LLZO800 cathode provided a discharge capacity of 135 mAh g^{-1} with a capacity retention of 92 % (cf. Fig. 8(k) and (l)).

Overall, coating performance via sol-gel can enhance the electrochemical performance of the LIBs especially in the cycling performance. Sol-gel coatings can provide a conformal and uniform coating on the surface of the cathode material, ensuring efficient utilization of the active material. This uniform coating can also minimize side reactions and degradation processes, thus can extend the cycle life of the battery. Again, it needs to be highlighted that, the sol-gel technique possesses multiple steps from sol formation, gelation, and drying, which can be time-consuming and require careful control of various parameters such as temperature, pH, and drying conditions. This complexity can increase the manufacturing cost and limit scalability. Maintaining the quality, uniformity, and reproducibility of the coatings can become more difficult as the batch size increases. This limitation can hinder commercialising the sol-gel-coated cathode materials. The sol-gel process also may not be suitable for all cathode materials. Some materials may undergo undesirable reactions or phase transformations during the coating process, leading to the formation of unwanted by-

Case 2:24-cv-10546-BRM-KGA ECF No. 30-48, PageID.4746 Filed 11/25/24 Page 30 of 69

products or a decrease in the electrochemical performance. The compatibility between the sol-gel technique and specific cathode materials needs to be carefully evaluated.

2.3. Solid-state reaction

The solid-state reaction method is the conventional method to prepare lithium-ion battery cathode materials. It is the simplest route to synthesize NMC material. In the solid-state reaction, the reactants in the form of powders or inorganic salts are thoroughly mixed and ground. The solid-state method is also used as a subsequent step in which the prepared NMC precursor via wet synthesis is mixed with Li salt. During mixing, these reactants come into close contact with one another, promoting atom or ion diffusion. Then, they are generally pressed into pellets to reduce the interatomic spacing for better rearrangement of atoms during sintering process. During the sintering/annealing process, the lithium and transition metal atoms arrange themselves into a new solid phase called a layered structure [10].

Solid-state reaction synthesis offers a few advantages over wet-chemical synthesis. It typically involves less steps, simpler equipment, and more straightforward processing route. It can yield high-purity materials since there is minimal contamination from solvents or by-products. Therefore, it is easier to scale up for industrial production due to its simplicity.

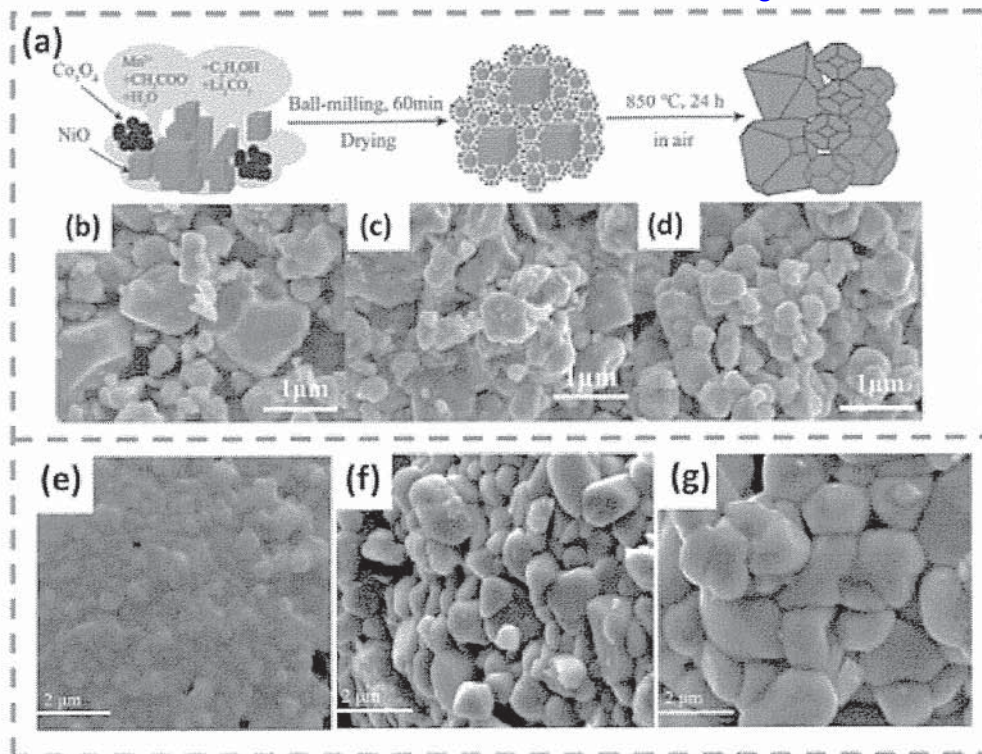
2.3.1. Effect of synthesis parameter

Pressure, temperature, and reaction time are critical parameters in solid-state reaction. High pressure applied during the mixing process improves reaction kinetics by increasing the contact area and density of the reactants, reducing void spaces, and enhancing homogeneity. High temperature enhances the mobility of atoms or ions, promoting diffusion and reaction rates. Reaction time is important for allowing sufficient diffusion and reaction to occur. However, excessive pressure can cause phase transition and defect formation [90]. In addition, excessive temperature and long reaction time during sintering process can cause a significant lithium loss and formation of large particles, resulting in the increasing length of Li ion diffusion path [91].

In the solid-state reaction, the solid reactants can be manually ground via mortar and pestle [92] or automated via ball-mills and planetary mills machines [93,94]. However, automatic grinders provide significant advantages over manual grinding methods. They allow more precise control over the grinding process, making them more effective and efficient in obtaining consistent results. However, when the solid-state reactions are conducted via milling machines, it is important to consider these factors to achieve desired reaction

outcomes [95]: 1) Milling time; longer milling periods allow more collisions and contacts between reactant particles, which promotes the reaction. 2) Milling speed; the rotational speed of the ball mill, can affect the intensity of impact exerted onto the reactant particles. Higher milling speeds result in more vigorous milling action, enhancing the reaction rates. 3) Ball-to-powder ratio; a higher ball-to-powder ratio provides more collisions between the balls and the reactant particles, enhancing the milling action and reaction rates. 4) Ball media and size; different media materials and sizes can affect the milling efficiency and collision frequency. 5) Atmosphere and environmental conditions; inert gas atmospheres can prevent unwanted reactions between the reactants with moisture or air. Therefore, the sample preparation and sealing of the mill jar are commonly done in an argon atmosphere [96].

The properties of the reactant materials, such as their composition, crystal structure, and solvent solubility, can affect the solid-state reactions [22,97]. Wang et al. [22] synthesized NMC 622 via a ball-mill assisted solid-state method as illustrated in Fig. 9(a). In their study, different types of manganese sources such as MnO_2 , Mn_3O_4 , and $\text{Mn}(\text{CH}_3\text{COO})_2$ were used. For simplification, the samples were labelled as M1, M2, and M3, respectively. The XRD analysis indicated that all XRD peaks obtained from the samples can be well-indexed to a hexagonal lattice of $\alpha\text{-NaFeO}_2$ -type layered structure, space group $R\bar{3}m$. The M3 sample possessed the largest $I(003)/I(104)$ ratio value which reflects a low degree of $\text{Ni}^{2+}/\text{Li}^+$ cation mixing. The SEM images of M1 and M2 particles exhibited irregular surfaces and severely agglomerated morphology, respectively (cf. Fig. 9(b) and (c)). On the other hand, M3 particles had regular morphology with octahedral crystal structure and quasi-spherical shape (cf. Fig. 9(d)). The authors claimed that the good morphology of M3 was due to good solubility of $\text{Mn}(\text{CH}_3\text{COO})_2 \cdot 4\text{H}_2\text{O}$ in ethanol solution which can easily reach the surface of other reactant materials. This helps to reduce their surface energy and dissociate the agglomerated particles. The M1, M2, and M3 cathodes produced first discharge capacity of 148.1, 160.5, and 163.6 mAhg^{-1} at 0.1C, respectively, and capacity retention of 89.6, 96.0, and 99.1 % after 100 cycles, respectively. Thus, the superior electrochemical performance of M3 cathode was due to its good morphology and insignificant cation mixing.



Download : Download high-res image (596KB)

Download : Download full-size image

Fig. 9. (a) Schematic illustration of synthesis of NMC622 by solid-state method, SEM images of NMC 622 (b) M1, (c) M2, and (d) M3. Reprinted with permission from Ref. [22], Copyright 2020 Elsevier. SEM images of NMC 811 calcined at (e) 750 °C, (f) 800 °C, and (g) 850 °C for 10h. Reprinted with permission from Ref. [98], Copyright 2021 Wiley.

The additives or catalysts can be introduced during ball milling to promote or control the solid-state reactions. Jiang et al. [94] studied the effect of citric acid as the chelating agent and PVP as the additive in solid-state reaction synthesis. A stoichiometric amount of metal acetate-based salts with citric acid and polyvinyl pyrrolidone (PVP) were mixed by high-energy ball milling and was named CP. For comparison, the samples were also prepared without PVP and without both citric acid and PVP, and were named CA and NC, respectively. The CP exhibited the highest discharge capacity at 173 mAhg^{-1} , followed by CA and NC with 143 and 123 mAhg^{-1} , respectively. The author claimed that the addition of citric acid enhanced the ordering degree of cation mixing, whereas the addition of PVP led to a greater crystallinity and better homogeneity of the particle size distribution.

Temperature and heating duration during sintering/calcination are important in solid-state reactions. The choice of temperature affects the activation energy required for the reaction to occur and influences the diffusion of atoms or ions within the solid materials. Whereas adequate heating duration provides sufficient time for diffusion and rearrangement of

atoms or ions. He et al. [98] studied the effect of calcination temperature from 750 to 850 °C for 10 h on the prepared NMC 811 samples via nano-grinding-assisted solid-state method. The choice of sintering temperature can affect the degree of $\text{Li}^+/\text{Ni}^{2+}$ cation mixing, crystal growth (cf. Fig. 9(e)–(g)), grain size, and specific surface area, and therefore the electrochemical performances of the prepared cathode materials. The sample sintered at 800 °C exhibited the best electrochemical performance with an initial discharge capacity of 203 mAhg^{-1} at 0.1 C and 91.8 % retention of capacity.

Generally, in solid-state reaction synthesis, a stoichiometric amount of inorganic metal salts and lithium salt were mixed and ground together. The choice of precursor can slightly affect the electrochemical performance [22,97]. The incorporation of organic additives during the mixing process can further aid the solid-state reactions. Other organic additives, including urea, oxalic, tartaric, and citric acid, have reportedly been used in the synthesis of NMC-based cathode materials via solid-state reaction [92,99]. Besides the organic additives, solvents such as ethanol or acetone are commonly added as dispersing agents in the solid-state reaction [95]. They wet the surfaces of the particles, reducing the attractive forces between them, and reducing the aggregation of particles [100]. Therefore, they improve the mixing homogeneity. Temperature and heating duration are critical factors in various synthesis techniques of cathode materials for LIBs as well as solid-state reaction method. A statistical study by Malik et al. [10], found that the NMC materials synthesized by a solid-state reaction required the highest energy for sintering process. This is because lithium and transition metal atoms must travel over large distances in solid phases, and require a long time to reach an equilibrium state. Therefore, it is important to optimize the desired temperature and duration of the sintering process as excessive temperature and heating duration can lead to significant lithium loss, promote $\text{Li}^+/\text{Ni}^{2+}$ cation mixing, and increase energy consumption.

2.3.2. Modification via solid-state reaction

2.3.2.1. Doping

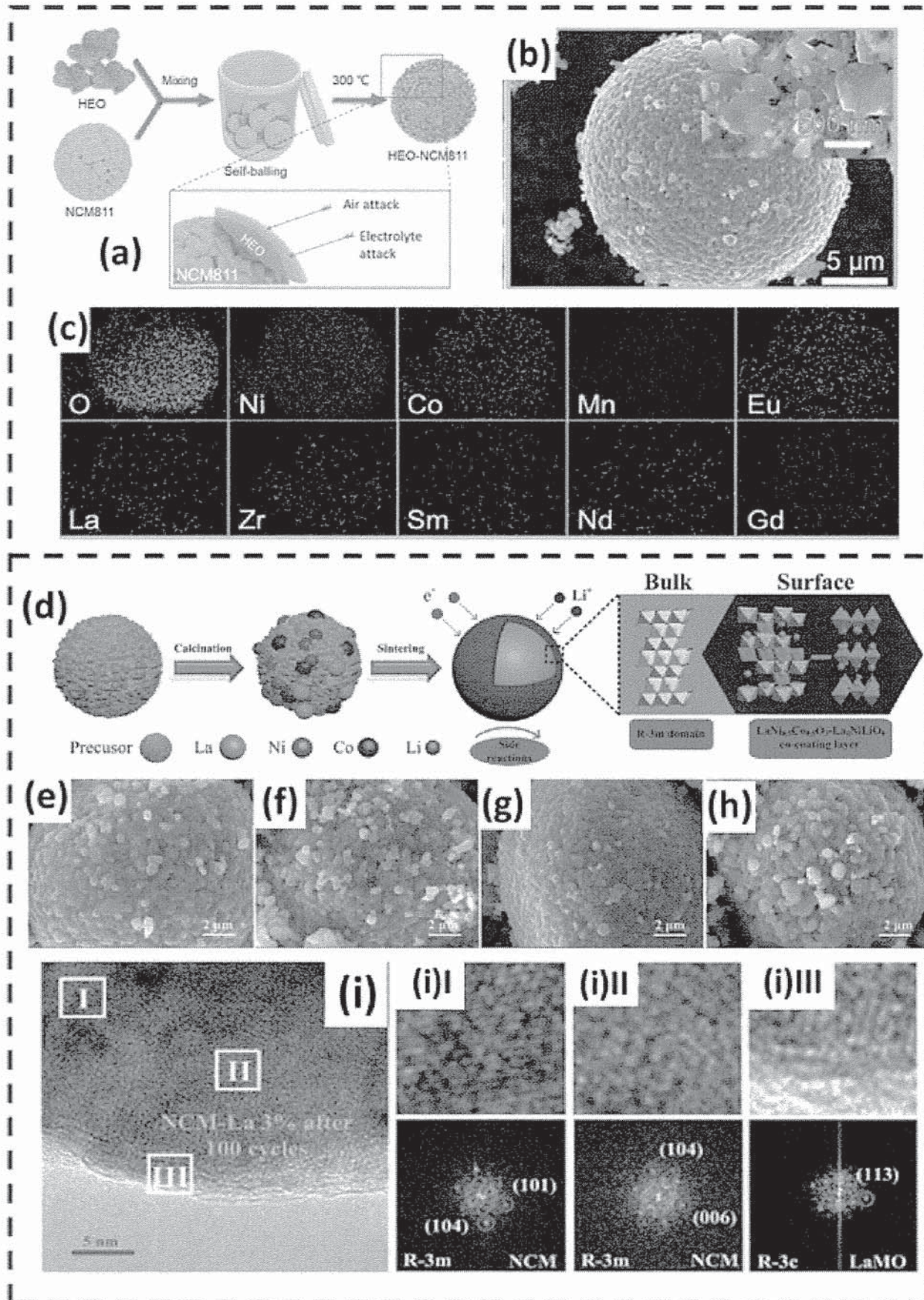
In a solid-state reaction, the doping salts are added together with other solid reactants during the mixing process before undergoing the heating process. Liu et al. [40] used ZrO_2 nanopowder as a dopant source in NMC 622. The NMC precursor, Li_2CO_3 , and ZrO_2 were mixed with a molar ratio of 1:0.54:0.01, respectively, followed by the sintering processes. The XRD peaks obtained from both samples can be well-indexed to an $\alpha\text{-NaFeO}_2$ -type layered structure. Evidence from XRD refinement suggested that the lattice parameter increased after Zr doping. The XPS confirmed the presence of Zr element and the EDX

confirmed the presence of Zr in the bulk structure of NMC. The Zr-doped NMC exhibited a slightly low initial discharge capacity at 55 °C with 196.5 mAh g⁻¹ when compared to pristine NMC with 201.3 mAhg⁻¹ at 1C. The lower initial discharge capacity of Zr-doped NMC is because of an inactive Zr element that does not contribute to the electrochemical reaction. However, Zr-doped NMC possessed much superior cycling performance with 98% capacity retention after 50 cycles when compared to pristine NMC with only 91%. This is because Zr doping enhances the structural stability of NMC materials owing to the strong Zr–O bond and low Li⁺/Ni²⁺ cation mixing.

2.3.2.2. Coating

The coating via solid-state reaction typically involves direct reaction of NMC powder and coating materials through mixing and grinding processes and followed by a heating process at elevated temperature. These processes are simpler and require fewer processing steps compared to other wet-coating methods.

Yuan et al. [101] studied the effectiveness of high entropy oxide (HEO) as coating materials for NMC 811. The (La_{0.2} Nd_{0.2} Sm_{0.2} Eu_{0.2} Gd_{0.2})₂ Zr₂O₇ HEO coating material was first prepared by mixing the La₂O₃, Nd₂O₃, Sm₂O₃, Eu₂O₃, Gd₂O₃, and ZrO₂ and followed by sintering process at 1300 °C. The HEO coating material was coated on NMC 811 at different weight ratios of 1, 3, 5, and 10wt% on NMC 811 via ball-milling. Finally, the mixtures were sintered at 300 °C in air for 1 h as illustrated in Fig. 10(a). Fig. 10(b) and (c) show the FESEM images of HEO nano-flakes that appeared on the surface of NCM811 and the EDX mapping further confirmed the presence of each coating element (Zr, Nd, Eu, Sm, La, and Gd), respectively. The 1.0wt% HEO displayed a higher initial discharge capacity with 194.7 mAhg⁻¹ than that of pristine NMC with 190.5 mAh g⁻¹ at 0.1C. Further increases in HEO coating materials displayed a decreasing trend in initial discharge capacity. The 5.0wt % HEO coated NMC 811 displayed the best retention capacity with 74.2 % for 300 cycles compared to pristine NMC 811 with only 57.3 %.



Download : Download high-res image (2MB)

Download : Download full-size image

Fig. 10. (a) Schematic illustration of coating process of NMC 811 with HEO, (b) SEM images of HEO coated NMC 811, and (c) EDX mapping of the HEO coated NMC 811 [101]. (d) Schematic illustration of La-surface coating on NMC material, SEM images of (e) NMC, (f) 1 % La-coating, (g) 3 % La-coating, and (g) 5 % La-coating on NMC, HRTEM and corresponding FFT images of (i) 3 % La-coating on NMC after 100 cycles. Reprinted with permission from Ref. [102] Copyright 2020 Elsevier.

Li et al. [102] prepared different molar ratios of La-coating material on NMC cathode material. The samples were first prepared by mixing NMC precursor, Li_2CO_3 and $\text{C}_6\text{H}_9\text{O}_6\text{La}\cdot x\text{H}_2\text{O}$ in a molar ratio of 2:1.05: (0.02, 0.06, and 0.1), respectively before heating processes as illustrated in Fig. 10(d). The XRD analysis indicated that all peaks obtained from the coated and pristine samples can be well-indexed to a hexagonal lattice of $\alpha\text{-NaFeO}_2$ -type layered structure, space group R-3m. The coated samples displayed some additional peaks that can be indexed to $\text{LaNi}_{0.5}\text{Co}_{0.5}\text{O}_3$ and $\text{La}_4\text{NiLiO}_8$ phases. The SEM images displayed small white particles which may imply the formation of La-based oxides covering the surface of NMC particles (cf. Fig. 10(e–h)). The coated sample with 3 % La-coating material exhibited a better retention capacity with 77% retention after 100 cycles when compared to pristine NMC with only 63%. Post-cycling diagnosis on coated NMC cathode through HRTEM analysis in Fig. 10(i(I)–(III)) display that the bulk and middle area retained the R-3m structure and the $\text{La}_4\text{NiLiO}_8$ phase belonged to the coating material on the NMC surface was well preserved. Whereas the bulk and middle area of the pristine sample evolved into the Li_2NiO_2 phase. Therefore, the coating layer successfully protected the inner NMC structure during cycling.

The simple process of coating via solid-state reaction through mechanical mixing and heating is advantageous for scaling up production. However, the prolonged and vigorous mixing process of the post-annealing NMC material can result in structural degradation, particle cracking, and induce phase transitions at the particle surface [103,104]. Therefore, careful selection of parameters during the mixing process is crucial for maintaining a good morphology and high quality of the layered structure of NMC material. The subsequent heating process is another crucial part of the coating process which promotes a solid-state reaction between the coating material precursor and the surface of the cathode material. The high elevated temperature can promote atom diffusion of coating material into the bulk of NMC and enhance the adhesion of coating material with the NMC [34]. However, the use of excessive temperature and long heating duration can cause a significant lithium loss and promote $\text{Li}^+/\text{Ni}^{2+}$ cation mixing which can deteriorate the electrochemical performance. This dry coating technique also comes with a few disadvantages such as limited coating thickness control and uneven coating distribution on the NMC surface.

2.4. Hydrothermal

The term hydrothermal method refers to the heterogeneous reaction for synthesizing inorganic materials in which the reaction takes place in fluids like water, aqueous solutions, and steam at specific temperatures and pressures [105,106]. The properties of water, such as density and dielectric constant, exhibit variations in response to changes in temperature and pressure. These variations could influence the process of nucleation, so enable the manipulation of crystal phase and particle size [105]. The hydrothermal process is very different from other synthesis methods due to the requirement for the reaction to occur within a sealed container called an autoclave, wherein crystal formation occurred. The autoclave is subjected to elevated temperatures that surpass the boiling point of the solvent. Supercritical fluids are generated through the application of high pressure and temperature, resulting in enhanced solubility of solid precursors. Consequently, this heightened solubility facilitates the subsequent precipitation and development of crystalline solids [107].

Synthesis via hydrothermal is a straightforward process. First, the stoichiometric amounts of inorganic metal salts or metal alkoxides are dissolved in distilled water under continuous stirring. Besides that, ammonium hydroxide is added as a pH regulator, whereas urea or ethanolamine is added as a precipitating agent. The prepared solution is then transferred into a Teflon-lined steel autoclaved, which is then sealed and subjected to heating at temperatures ranging from 100 to 250°C for an extended duration. This process often results in the formation of a colourless, clear solution accompanied by the appearance of a brown precipitate. The precipitates that were acquired are subjected to rinsing, filtration, and drying processes. The dried powder is then mixed with lithium salts and finally subjected to sintering process. The products obtained from this synthesis method often result in high-purity materials and good crystallinity. They are also highly reproducible in terms of purity, crystallinity, and morphologies [108]. However, a major disadvantage of this method is the inability to produce large quantities of the products in a single run.

2.4.1. Effect of synthesis parameter

The synthesis of the product using this approach can be influenced by various factors, such as hydrothermal temperature and duration, the molar ratio of precipitating agent to transition metal ions, type of solvent, reactant concentration, and pH value. Therefore, it is necessary to carefully regulate the process conditions during the reaction.

In a study conducted by Yang Shi et al. [109], it was shown that the utilization of an alternative time duration for the hydrothermal reaction, specifically 30h, did not significantly improve the cycle stability of the cathode material when compared to a

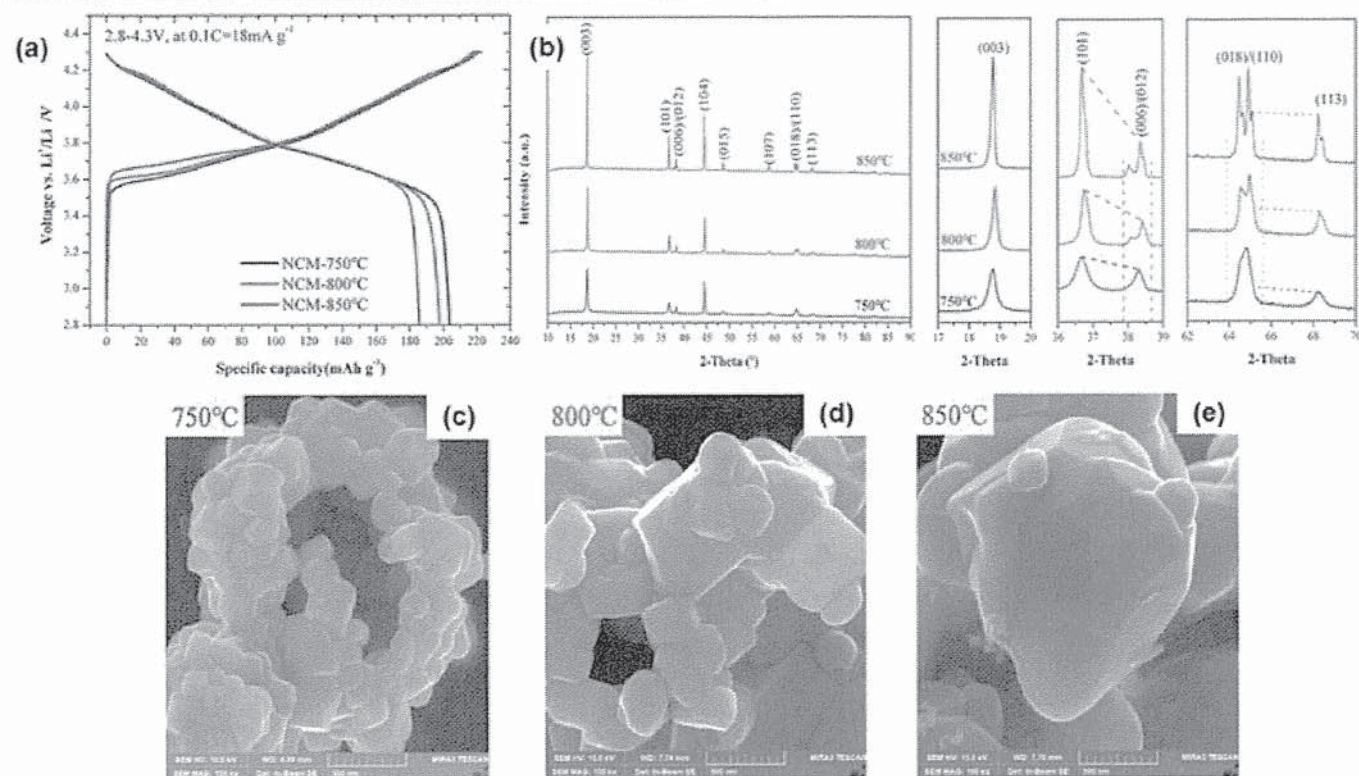
reaction duration of 24h. Nevertheless, the evaluation of a lengthier reaction time proves to be a laborious task, and the enhancement in electrochemical performance is minimal. Consequently, it is postulated that a hydrothermal reaction lasting 24h represents the most favourable condition for synthesizing precursors using this methodology. Li et al. [110] noticed similar observations in their study, wherein the $\text{LiNi}_{0.7}\text{Co}_{0.15}\text{Mn}_{0.15}\text{O}_2$ samples were synthesized with varying reaction times. The findings demonstrate that the utilization of a 24-h time frame yields better cyclability and rate capability.

Urea is frequently employed as a precipitating agent in hydrothermal processes. It slowly decomposes to produce carbonate ions (CO_3^{2-}) as precipitating agents in the reaction mixture, permitting particle ripening during precipitation. Yang Shi et al. [109] studied the effect of the mole ratio of urea with transition metals (2:1, 5:2, and 3:1) in hydrothermal synthesis of NMC 532 precursor at 200°C for 12h. The 5:2 ratio is the optimum ratio to obtain the target stoichiometry composition of NMC 532. The importance to optimize this ratio is due to the differences in the equilibrium constant between each element reaction. The equilibrium constant (K_{sp}) of manganese carbonate, cobalt carbonate and nickel carbonate are 8.8×10^{-11} , 1×10^{-10} and 1.4×10^{-7} , respectively. This makes the manganese the easiest to be precipitated. It is reported that the undesirable stoichiometry in high (3:1) and low ratios (2:1) results from the competition between the carbonate precipitation formation and the production of ammonia complexes. The NH_4^+ ions, which was released from the urea decomposition could react with transition metal ions to form soluble ammonia complexes $[\text{M}(\text{NH}_3)_n]^{2+}$, where $\text{M} = \text{Ni}, \text{Co}, \text{and Mn}$. The optimised sample of NMC 532 with the mole ratio of urea with transition metals (5:2) and hydrothermal at 200°C for 24h delivers the highest discharge capacity of 161.7 mAhg^{-1} .

Zhang et al. [30] synthesized NMC811 via a hydrothermal route. They reported on the effect of sintering temperature on the electrochemical performances and the crystalline structure. The sintering temperatures were chosen at 750°C , 800°C , and 850°C and the samples were labelled as NMC- 750°C , NMC- 800°C , and NMC- 850°C , respectively. It is reported that the NMC- 750°C has the highest discharge capacity at 0.1 C of 203.7 mAhg^{-1} as shown in Fig. 11(a). It is also found that after 200 cycles, the capacity retention of NMC- 750°C remained at 86.2 % of its initial discharge capacity at 0.1 C. Fig. 11(b) represents the diffraction patterns of NMC- 750°C , NMC- 800°C , and NMC- 850°C . It is safe to conclude that as the sintering temperature increases, the splitting peaks (006)/(012) and (018)/(110) are getting obvious due to the well-ordered layered structure. The SEM images of all samples are demonstrated in Fig. 11(c)–(e). The elevated sintering temperatures significantly affected the particle size of the samples which the samples became larger with temperature. The NMC- 750°C

Case 2:24-cv-10546-BRM-KGA ECF No. 30-48, PageID.4755 Filed 11/25/24 Page 39 of 69

exhibited good electrochemical performances because the small particles of NMC-750°C can fully maximize the lithium ions diffusion.



Download : Download high-res image (813KB)

Download : Download full-size image

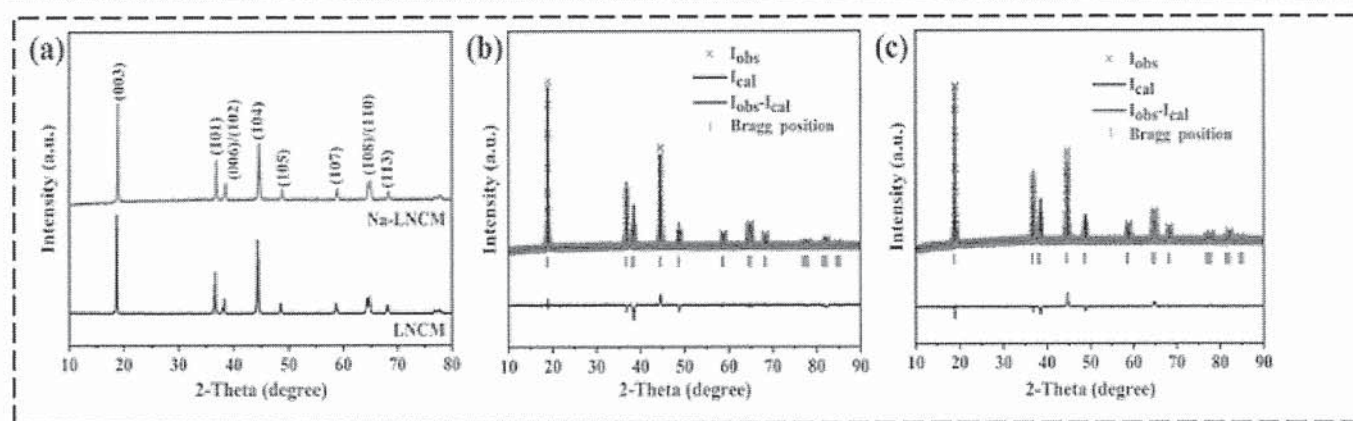
Fig. 11. (a) Charge/discharge curve at 0.1 C rate, (b) XRD patterns, and SEM images of samples sintered at (d) 750, (d) 800, and (e) 850°C. Reprinted with permission from Ref. [30], Copyright 2020 Elsevier.

The hydrothermal process is characterized by a unique method, as it involves the use of an autoclave for the reaction. However, the procedural steps have a few similarities to those employed in co-precipitation and sol-gel procedures. In hydrothermal processes, chelating agents are commonly employed to improve the properties of cathode materials. Urea is frequently employed as a chelating agent due to its ability to release CO_3^{2-} during thermal breakdown at elevated temperatures. Additional examples of chelating agents employed in hydrothermal processes are oxalic acid, lithium hydroxide monohydrate, and ammonium bicarbonate [10]. Based on the observations made by earlier researchers, it is commonly observed that hydrothermal processes typically include varying durations, with researchers often opting for overnight or 24-h reaction periods due to the favourable product outcomes.

2.4.2. Modification via hydrothermal

2.4.2.1. Doping

Liu et al. [111] doped the NMC precursor with Na via hydrothermal method. The precursor was dispersed in a 50mL NaOH solution with Na:Transition metal ion ratio of 0.03:1, respectively. Fig. 12(a) shows the XRD patterns of both samples displayed a typical hexagonal α -NaFeO₂ layered structure with space group R-3m. Rietveld refinement analysis as in Fig. 12(b) and (c) confirmed that the Na⁺ is introduced into the lithium layer and broadened the spacing of the Li slab. The Na-doped NMC displayed better electrochemical performances in terms of cycling and rate performance. This is because Na ions inhibited the mixing of Li⁺/Ni²⁺ cations and expanded the diffusion channels of Li⁺.



Download : Download high-res image (466KB)

Download : Download full-size image

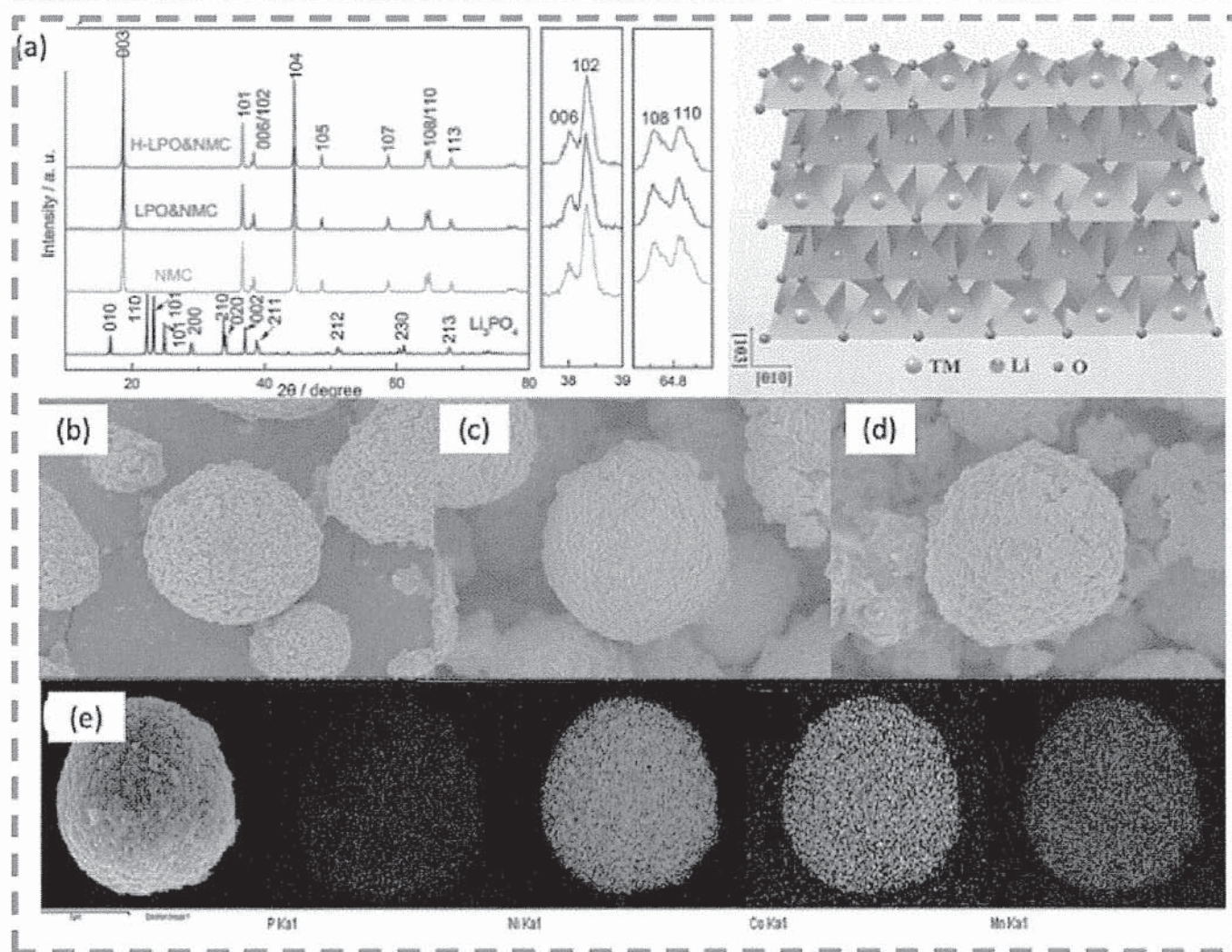
Fig. 12. XRD pattern of (a) LNCM and Na-LNCM, and Rietveld refinement of (b) LNCM (c) Na-LNCM sample. Reprinted with permission from Ref. [111], Copyright 2023 Elsevier.

2.4.2.2. Coating

Yuan et al. [44] prepared the Li₃PO₄ (LPO) coated LiNi_{0.8}Mn_{0.1}Co_{0.1}O₂ via hydrothermal method. The NMC precursor, PVA, (NH₄)₂HPO₄, and LiOH were mixed in deionized water and hydrothermal at 180°C for 24h and followed by sintering process. The sample was named H-LPO&NMC. Whereas the LPO&NMC and NMC were named after the coated sample prepared without hydrothermal treatment and NMC 811 without coating, respectively. Fig. 13 (a) displays all XRD patterns, and the samples exhibited layered hexagonal α -NaFeO₂ structure with R3-m space group. Fig. 13(b), (c), and (d) show all the samples exhibited the same spherical particle which mean that the hydrothermal treatment process did not influence the morphology of final products. The EDS mapping of the H-LPO&NMC shows that the P element from LPO was well distributed on the NMC particle (cf. Fig. 13(e)). The H-LPO&NMC delivered an initial discharge capacity of 210 mAhg⁻¹ with 92.6% capacity

Case 2:24-cv-10546-BRM-KGA ECF No. 30-48, PageID.4757 Filed 11/25/24 Page 41 of 69

retention whereas the NMC sample possessed 199 mAhg^{-1} , with retention of only 84 % at 50 cycles. The good ionic conductivity and chemical stability of LPO contributed to the improved electrochemical performances of the H-LPO&NMC. Besides, the coating layer provided SEI resistance and therefore minimised the side reactions of the active material with electrolytes.



Download : Download high-res image (1MB)

Download : Download full-size image

Fig. 13. (a) XRD patterns of the NMC, LPO&NMC, H-LPO&NMC and Li_3PO_4 , HRSEM images of (b) NMC, (c) LPO&NMC and (d) H-LPO&NMC, and (e) EDS mapping images. Reprinted with permission from Ref. [44], Copyright 2019 Elsevier.

The coating technique via the hydrothermal method is a well-known technique to provide a thin and uniform coating layer on the cathode surface. However, the vigorous reaction from the hydrothermal process due to the high pressure and temperature can potentially degrade the crystalline structure and induce the morphology of the bulk NMC cathode materials. In

addition, the Ni-rich NMC cathode materials are moisture sensitive, and the water will extract lithium from the lattice causing structural damage [112]. Therefore, the coating technique proposed by Yuan et al. [44], by mixing the NMC precursor, and coating precursor in Li source solution for the hydrothermal process is one way to avoid these issues. The coating technique via the hydrothermal method can provide a huge challenge for large-scale production due to the intricate process requirements and the need to maintain consistent coating quality across a larger volume of materials.

2.5. Combustion

The NMC cathode materials can be conveniently and effectively prepared by the combustion method. In the direct combustion method, the metal alkoxides or the inorganic metal salts are first measured according to stoichiometric proportions and dissolved in deionized water. These metal salts act as oxidants in the combustion reaction. Fuel such as citric acid is also dissolved in the mixture solution and thoroughly stirred for homogeneity. Subsequently, the solution is heated at temperatures ranging from 100 to 400°C, which led to spontaneous combustion of the mixture and ended with the formation of dried powders. Finally, these powders are subjected to calcination process.

The combustion method presents numerous benefits, such as simplicity, convenience, cost-effectiveness, rapid heating rates, and short processing time. Additionally, it allows for easy control over the chemical composition, morphology, and crystallite size of the materials. As a promising technique for preparing cathode materials, it strikes a balance between efficiency, cost-effectiveness, and controllability, making it appealing for diverse applications in energy storage and other fields. The combustion method primarily relies on three key constituents: the oxidizer, fuel, and solvent.

2.5.1. Effect of synthesis parameters

Different metal inorganic salts, including metal nitrates, carbonates, and acetates, can serve as oxidants. Among these salts, nitrates are the most utilized due to several advantageous features. Nitrates are preferred as oxidizers in the combustion method for several reasons. 1) They are cost-effective and widely available. 2) They are low toxicity making them safer to be handled. 3) They exhibit a higher oxygen content, which aids in the exothermic combustion process, leading to rapid formation of desired cathode materials. 4) They have relatively low decomposition temperatures, ensuring easy release of oxygen during heating, thus promoting efficient and controlled combustion. 5) Good solubility in water, enabling straightforward dissolution and homogeneous mixing with other raw materials. The combination of these features, such as high oxygen content, ease of decomposition,

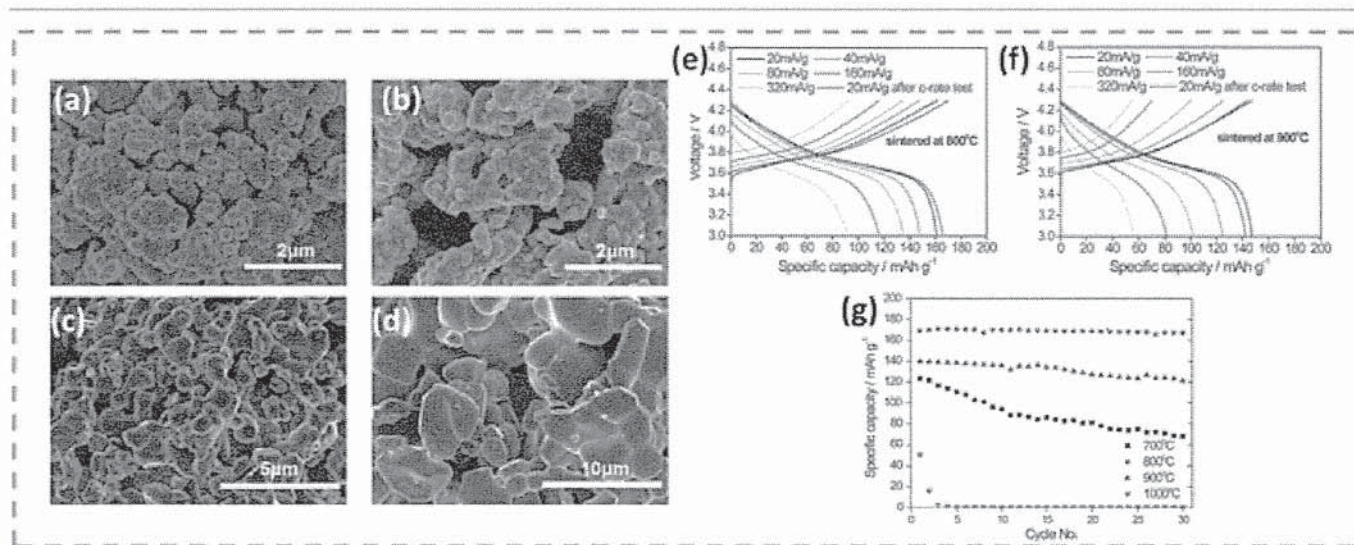
homogeneity, versatility, compatibility with aqueous solutions, low toxicity, and cost-effectiveness, makes metal nitrates the preferred choice as oxidizers in the combustion method for cathode materials synthesis [113].

The selection of fuels in the combustion method for cathode materials plays a crucial role in determining the synthesis process and the properties of the resulting materials. Different fuels can affect the combustion temperature, combustion rate, and chemical composition of the cathode materials. When choosing fuels, certain factors become essential, such as cost-effectiveness, stability, ease of handling, minimal environmental impact, and the ability to produce homogenous and pure materials. The fuel is selected from a variety of reducing agents including urea, glycine, citric acid, hydrazine, and starch. Urea is the preferred choice of fuel for combustion because it is cheaper, easily available, and water-soluble. Meanwhile, citric acid has also been reported to be a good complexing agent and eco-friendly fuel that can improve the LIB electrochemical performances [114]. In a different study [115], NMC cathode materials were synthesized using different fuels such as glycine, tartaric acid, and citric acid. Among the tested fuels, tartaric acid demonstrated the highest discharge capacity of 185.9 mAh g^{-1} compared to glycine and citric acid. On the other hand, Elong et al. [116] conducted a separate investigation on the electrochemical performance of NMC cathode materials synthesized through the combustion method. In their study, different fuels such as citric acid, urea, and glycine were employed, and water was used as the solvent. Their findings revealed that NMC cathode materials synthesized with citric acid exhibited the highest discharge capacity of 130.80 mAhg^{-1} . The good performance was attributed to low cation mixing, higher crystallinity, and smaller crystallite size compared to materials synthesized using glycine and urea as fuels. The research study demonstrated that the choice of fuel in the combustion method significantly influenced the structure, crystallite size, and overall performance of the cathode materials. Both studies highlighted the significance of fuel and solvent selection in the combustion method for synthesizing NMC cathode materials and their direct impact on the electrochemical performance of the prepared cathode materials.

The selection of the solvent in the combustion method depends on several crucial factors, including its ability to dissolve the raw materials and fuel, ensuring high purity to prevent the introduction of impurities during the process, safety during handling, low toxicity, non-flammability, and minimal environmental impact. These considerations aim to obtain high-quality cathode materials suitable for various applications. Common solvents used include water, ethanol, methanol, acetone, and their mixtures. Among these options, water stands out due to its wide availability, excellent dissolution capacity for various reactants, safety features, and environmentally friendly characteristics. These attributes make water a

preferred and versatile solvent for synthesizing cathode materials through the combustion method. Overall, careful consideration of solvent choice is crucial in optimizing the synthesis process and achieving the desired properties of the cathode materials.

Ahn et al. [26] studied the effect of annealing temperature from 700 to 1000°C on the performance of the NMC622 materials. The cathode materials were synthesized using the simple combustion method and urea was used as a fuel. The morphologies of the synthesized NMC622 at different annealing temperature are shown in Fig. 14(a) and (b), 14(c) and 14(d) for 700, 800, 900 and 1000°C, respectively. These figures show that the morphologies of the synthesized samples were strongly dependent on the annealing temperature. NMC622 annealed at 800°C exhibited a discharge capacity of 170.1 mAh g⁻¹ with 98.2 % capacity retention after 30th cycles, as shown in Fig. 14(e) and (g). The excellent performance of this material was due to the higher crystallinity, well-organized layered structure with a higher ratio of c/a, shorter diffusion, and uniform distribution nanoparticles. Whereas the NMC622 synthesized at 900°C shows a drop in performance with a lower first discharge capacity, rate capability, and capacity retention as shown in Fig. 14(f) and (g) due to lower ratio of c/a and larger particles.



Download : Download high-res image (640KB)

Download : Download full-size image

Fig. 14. FESEM images of NMC622 sintered at (a) 700, (b) 800, (c) 900 and (d) 1000°C; Charge-discharge curves at different current density of NMC 622 sintered at (e) 800 and (f) 900°C; (g) Cyclic performance. Reprinted with permission from ref (Ahn et al., 2014), Copyright 2014 Elsevier.

In conclusion, careful consideration of the main elements, such as the types of oxidants, fuels, and solvents, is essential for researchers when using the combustion method to synthesize cathode materials. These key components significantly influence the structure, morphology, particle size, and electrochemical performance of the cathode materials. The combustion method offers tuneable parameters, including the fuel-to-oxidizer ratio, fuel mixture, and sintering process, which can be utilized to control and optimize the characteristics of the cathode materials. Precise calculations of the fuel and oxidizer quantities are crucial for achieving structural stability, desired material morphology, appropriate crystallite size, and avoiding excessively vigorous reactions during the synthesis process. Optimizing the annealing process can provide valuable insights into the parameters that yield the best performance for cathode materials. Understanding these conditions can offer significant advantages for the large-scale production of cathode materials used in LIBs.

2.5.2. Modification via combustion

2.5.2.1. Doping

Doping has been identified as an effective strategy to enhance structural stability, inhibit $\text{Li}^+/\text{Ni}^{2+}$ mixing, and improve the electrochemical performance of Ni-rich cathode materials. Various doping elements, including Aluminium and Titanium, have been successfully incorporated to achieve these improvements [117]. Conry et al. [118] conducted a study using Al as a dopant, but the result showed capacity fading in Ni-rich cathode materials. However, Ti doping via the combustion method proved to be more beneficial, as it enhanced the stability of the crystal structure and reduced cation mixing in the layered structure. This led to significantly improved cycling stabilities, with 91.9% capacity retention after 70 cycles at a 3C rate at room temperature [119]. These findings demonstrate that the doping strategy can significantly enhance the electrochemical performance of cathode materials synthesized using the combustion method.

3. Perspective

Progression towards a low-cost battery within the industry has seen a shift towards nickel-rich cathode materials. A greater understanding of NMC cathode materials is important to optimize the performance of LIBs. This paper provides a review on the influence of synthesis route and certain modifications on the NMC performance. Each synthesis method has its own advantages and disadvantages. Among all, the co-precipitation method can be considered as the most effective method to prepare NMCs for industrialization purposes.

This is due to the highly scalable and good homogeneity at the particle scale of the synthesis product, together with relatively simple and low-cost synthesis conditions.

The synthesized NMCs should yield good structural properties to produce a good electrochemical performance of LIBs. Therefore, it is important to anticipate the performance of NMC cathode materials from the obtained XRD data. The ideal structure of the synthesized NMCs should meet these three criteria: (1) high purity with no presence of contamination and other secondary phases, (2) the observable splitting of (006)/(012) and (018)/(110) peaks, which demonstrates the formation of well-ordered NMC layered structures, and (3) the high $I(003)/I(104)$ ratio, which reflects low Ni/Li cation mixing. Most of the reported works show outstanding electrochemical performances when these criteria are fulfilled [120,121]. However, fulfilling these criteria is challenging and it is a time-consuming process, where lots of tuning of the synthesis parameter are required.

The electrochemical performance of NMCs is affected by their morphology, including surface area and tap density. This morphology can be manipulated by tuning the synthesis parameter. The porous, small, and low agglomeration particles can give a high specific surface area which is good for electrode/electrolyte contact, and consequently, delivering high discharge capacity and rate performance; whereas the NMCs with a dense morphology can produce a high volumetric energy density [122]. Recently, the single-crystalline vs. poly-crystalline cathode has become a current topic in the battery research field. The use of single-crystalline NMCs is one of the promising approaches in solving the cycling stability issues as its morphology limits surface reactivity and particle cracking [112]. However, the synthesis process of single-crystalline NMCs is more complex than that of poly-crystalline. The high-temperature calcination approach can promote other structural disorders, whereas the molten-salt synthesis approach requires a lot of washing and rinsing processes. Therefore, a simpler synthesis approach is needed to produce high-quality single-crystalline NMCs.

The Ni-rich NMCs suffered from a quick cell failure due to some degradation factors. Therefore, techniques such as doping, and surface coating can be employed to further improve the electrochemical performance of NMC cathode materials. NMCs coated with other metal oxides are reported to have better electronic conductivity due to enhanced electron and Li transportation. Surface coating suppressed the side reaction between the electrode and electrolyte. However, constructing a uniform coating layer with an optimal thickness is a challenging task. Doping method improved the battery performances by improving the structural, electrochemical, and thermal properties. However, challenges in doping method are difficulty in obtaining single phase layered structure, distorted crystal

structure, increased mixed cation ratio and volumetric expansions. In addition, the complicated modification processes with high prices of machines and materials used may not be practical to the industries. Therefore, development of efficient, cheap, and simple modification techniques is vital to increase the mass production of Ni-rich NMCs.

Many modifications on the NMCs such as doping, coating, and single-crystalline morphology have been proven to improve the electrochemical performance of NMC cathode materials. However, more evidence is needed to gain a deeper understanding on the contribution of such modifications toward the performance of LIBs. Below are some advanced tools and methods that can be used to gain more understanding on the NMC cathode materials.

- (1) Computational analysis has become a good tool in studying LIBs. The design of a new material is challenging, but computational analysis provides microscopic details such as position of ions, parameters of crystal cell, stability information, electronic structure, doping sites, chemical activities of elements, intercalation potentials and possible Li-ion diffusion path. Therefore, recent material research combines with both experimental and computational investigations, is expected to bring further breakthroughs in the next generation of high-performance LIBs.
- (2) Research instruments such as XRD, optical microscopy, electron microscopy, Raman spectroscopy, and nuclear magnetic resonance have been designed to support in situ studies. The “in situ” means “in the original position or place,” whereas in scientific experimentation, it refers to the experiment carried out under real operating conditions. These studies can provide more insights on the structural evolution, formation of solid–electrolyte interphase, side reactions and redox mechanism as well as Li-ion transport properties during charge-discharge. These studies are important to further understand the operation of Li-ion batteries.
- (3) The purpose of failure analysis is to determine the primary cause(s) that leads to failure and then develop ways to prevent any future failure occurrence. This is important as LIB failure can cause fire and/or explosion which results in severe injuries to the user. Common failure analysis on NMC-based LIB has been reported such as undesirable side reactions at the interfaces of electrode and electrolyte, irreversible phase transformation, and formation of microcracks, which ultimately decrease the battery lifetimes. Therefore, certain modifications can be made to the NMCs with the aim to minimize these potential failures.

Data availability

Additional information

No additional information is available for this paper.

CRedit authorship contribution statement

Farish Irfal Saaid: Writing – review & editing, Writing – original draft. **Muhd Firdaus Kasim:** Writing – review & editing, Writing – original draft, Validation, Supervision, Project administration, Funding acquisition, Conceptualization. **Tan Winie:** Writing – review & editing. **Kelimah Anak Elong:** Writing – review & editing, Writing – original draft. **Azira Azahidi:** Writing – review & editing, Writing – original draft. **Nurul Dhabitah Basri:** Writing – review & editing, Writing – original draft. **Muhamad Kamil Yaakob:** Writing – review & editing. **Mohd Sufri Mastuli:** Writing – review & editing. **Siti Nur Amira Shaffee:** Writing – review & editing, Funding acquisition. **Mohd Zaid Zolkiffly:** Writing – review & editing, Funding acquisition. **Mohamad Rusop Mahmood:** Writing – review & editing.

Declaration of competing interest

The authors declare that they have no known competing financial interests or personal relationships that could have appeared to influence the work reported in this paper.


Acknowledgment

The authors would like to thank the Petronas Research Sdn. Bhd. (PRSB), Malaysia for the funding [Project File No. 20221011001], Faculty of Applied Sciences and Centre for Functional Materials and Nanotechnology, Institute of Science, Universiti Teknologi MARA, Shah Alam, Selangor, Malaysia for their support to this work.

Special issue articles Recommended articles

References

- [1] Y. Hua, X. Liu, S. Zhou, Y. Huang, H. Ling, S. Yang
Toward Sustainable reuse of retired lithium-ion batteries from electric vehicles
Resour. Conserv. Recycl., 168 (2021), Article 105249, 10.1016/j.resconrec.2020.105249 ↗

 [View PDF](#) [View article](#) [View in Scopus ↗](#) [Google Scholar ↗](#)

- [2] N.O. Kapustin, D.A. Grushevenko

Long-term electric vehicles outlook and their potential impact on electric grid

Energy Pol., 137 (2020), Article 111103, 10.1016/j.enpol.2019.111103 ↗

 [View PDF](#) [View article](#) [View in Scopus ↗](#) [Google Scholar ↗](#)

- [3] A.C. Mersky, F. Sprei, C. Samaras, Z. Sean, Qian

Effectiveness of incentives on electric vehicle adoption in Norway

Transp Res D Transp Environ, 46 (2016), pp. 56-68, 10.1016/j.trd.2016.03.011 ↗

 [View PDF](#) [View article](#) [View in Scopus ↗](#) [Google Scholar ↗](#)

- [4] S. Panchal, M. Mathew, R. Fraser, M. Fowler

Electrochemical thermal modeling and experimental measurements of 18650 cylindrical lithium-ion battery during discharge cycle for an EV

Appl. Therm. Eng., 135 (2018), pp. 123-132, 10.1016/j.applthermaleng.2018.02.046 ↗

 [View PDF](#) [View article](#) [View in Scopus ↗](#) [Google Scholar ↗](#)

- [5] Venditti Bruno, EVs vs

Gas Vehicles: what Are Cars Made Out of?

Elements (2022)

<https://elements.visualcapitalist.com/evs-vs-gas-vehicles-what-are-cars-made-out-of/> ↗, Accessed 12th Oct 2022

[Google Scholar ↗](#)

- [6] A. Manthiram

A reflection on lithium-ion battery cathode chemistry

Nat. Commun., 11 (2020), p. 1550, 10.1038/s41467-020-15355-0 ↗

[View in Scopus ↗](#) [Google Scholar ↗](#)

- [7] Jörn Jürgens

This Is Why NCM Is the Preferable Cathode Material for Li-Ion Batteries, LG Energy Solution Blog Europe

(2019)

<https://lghomebatteryblog.eu/en/this-is-why-ncm-is-the-preferable-cathode-material-for-li-ion-batteries/> ↗, Accessed 7th Oct 2022

[Google Scholar ↗](#)

[8] V. Chandran, A. Ghosh, C.K. Patil, V. Mohanavel, A.K. Priya, R. Rahim, R. Madavan, U.

Muthuraman, A. Karthick

Comprehensive review on recycling of spent lithium-ion batteries

Mater Today Proc, Elsevier Ltd (2021), pp. 167-180, 10.1016/j.matpr.2021.03.744 ↗

 View PDF View article View in Scopus ↗ Google Scholar ↗

[9] Venkat Viswanathan, Alexander Bills, Shashank Sripad

EV Battery Costs Explained _ Industrial Equipment News

(2020)

<https://www.iem.com/product-development/news/21141505/ev-battery-costs-explained> ↗,

Accessed 21st Feb 2023

Google Scholar ↗

[10] M. Malik, K.H. Chan, G. Azimi

Review on the synthesis of $\text{LiNi}_x\text{Mn}_y\text{Co}_{1-x-y}\text{O}_2$ (NMC) cathodes for lithium-ion batteries

Mater. Today Energy, 28 (2022), Article 101066, 10.1016/j.mtener.2022.101066 ↗

 View PDF View article View in Scopus ↗ Google Scholar ↗

[11] X. Zeng, M. Li, D. Abd El-Hady, W. Alshitari, A.S. Al-Bogami, J. Lu, K. Amine

Commercialization of lithium battery technologies for electric vehicles

Adv. Energy Mater., 9 (2019), Article 1900161, 10.1002/aenm.201900161 ↗

View in Scopus ↗ Google Scholar ↗

[12] S.G. Booth, A.J. Nedoma, N.N. Anthonisamy, P.J. Baker, R. Boston, H. Bronstein, S.J. Clarke, E.J.

Cussen, V. Daramalla, M. de Volder, S.E. Dutton, V. Falkowski, N.A. Fleck, H.S. Geddes, N.

Gollapally, A.L. Goodwin, J.M. Griffin, A.R. Haworth, M.A. Hayward, S. Hull, B.J. Inkson, B.J.

Johnston, Z. Lu, J.L. MacManus-Driscoll, X. Martínez De Irujo Labalde, I. McClelland, K.

McCombie, B. Murdock, D. Nayak, S. Park, G.E. Pérez, C.J. Pickard, L.F.J. Piper, H.Y. Playford, S.

Price, D.O. Scanlon, J.C. Stallard, N. Tapia-Ruiz, A.R. West, L. Wheatcroft, M. Wilson, L. Zhang,

X. Zhi, B. Zhu, S.A. Cussen

Perspectives for next generation lithium-ion battery cathode materials

Apl. Mater., 9 (2021), Article 109201, 10.1063/5.0051092 ↗

View in Scopus ↗ Google Scholar ↗

[13] A.W. Moses, H.G.G. Flores, J.-G. Kim, M.A. Langell

Surface properties of LiCoO_2 , LiNiO_2 and $\text{LiNi}_{1-x}\text{Co}_x\text{O}_2$

Appl. Surf. Sci., 253 (2007), pp. 4782-4791, 10.1016/j.apsusc.2006.10.044 ↗

 [View PDF](#) [View article](#) [View in Scopus](#) [Google Scholar](#)

- [14] J. Zheng, G. Teng, C. Xin, Z. Zhuo, J. Liu, Q. Li, Z. Hu, M. Xu, S. Yan, W. Yang, F. Pan
Role of superexchange interaction on tuning of Ni/Li disordering in layered
Li(NixMnyCoz)O2

J. Phys. Chem. Lett., 8 (2017), pp. 5537-5542, 10.1021/acs.jpclett.7b02498 [↗](#)

[View in Scopus](#) [Google Scholar](#)

- [15] X. Miao, H. Ni, H. Zhang, C. Wang, J. Fang, G. Yang
Li2ZrO3-coated 0.4Li2MnO3·0.6LiNi1/3Co1/3Mn1/3O2 for high
performance cathode material in lithium-ion battery

J. Power Sources, 264 (2014), pp. 147-154, 10.1016/j.jpowsour.2014.04.068 [↗](#)

 [View PDF](#) [View article](#) [View in Scopus](#) [Google Scholar](#)

- [16] R.M. Salgado, F. Danzi, J.E. Oliveira, A. El-Azab, P.P. Camanho, M.H. Braga
The latest trends in electric vehicles batteries

Molecules, 26 (2021), p. 3188, 10.3390/molecules26113188 [↗](#)

[View in Scopus](#) [Google Scholar](#)

- [17] C. Li, H.P. Zhang, L.J. Fu, H. Liu, Y.P. Wu, E. Rahm, R. Holze, H.Q. Wu
Cathode materials modified by surface coating for lithium ion batteries

Electrochim. Acta, 51 (2006), pp. 3872-3883, 10.1016/j.electacta.2005.11.015 [↗](#)

 [View PDF](#) [View article](#) [View in Scopus](#) [Google Scholar](#)

- [18] A. Chakraborty, S. Kunnikuruvan, S. Kumar, B. Markovsky, D. Aurbach, M. Dixit, D.T. Major
Layered cathode materials for lithium-ion batteries: review of
computational studies on LiNi1-x-yCoxMnyO2 and LiNi1-x-yCoxAlYO2

Chem. Mater., 32 (2020), pp. 915-952, 10.1021/acs.chemmater.9b04066 [↗](#)

[View in Scopus](#) [Google Scholar](#)

- [19] E.V. Database
Compare Electric Vehicles - EV Database UK

(2023)

<https://ev-database.org/uk/> [↗](#), Accessed 5th Mar 2023

[Google Scholar](#)

- [20] C. Liu, Z.G. Neale, G. Cao
Understanding electrochemical potentials of cathode materials in
rechargeable batteries

Mater. Today, 19 (2016), pp. 109-123, 10.1016/j.mattod.2015.10.009 ↗

 [View PDF](#) [View article](#) [View in Scopus ↗](#) [Google Scholar ↗](#)

- [21] L.M. Morgan, M.M. Islam, H. Yang, K. O'Regan, A.N. Patel, A. Ghosh, E. Kendrick, M. Marinescu, G.J. Offer, B.J. Morgan, M.S. Islam, J. Edge, A. Walsh
From atoms to cells: multiscale modeling of LiNixMnyCozO2 cathodes for Li-ion batteries

ACS Energy Lett., 7 (2022), pp. 108-122, 10.1021/acsenergylett.1c02028 ↗

[View in Scopus ↗](#) [Google Scholar ↗](#)

- [22] L. Wang, B. Huang, W. Xiong, M. Tong, H. Li, S. Xiao, Q. Chen, Y. Li, J. Yang
Improved solid-state synthesis and electrochemical properties of LiNi0.6Mn0.2Co0.2O2 cathode materials for lithium-ion batteries

J. Alloys Compd., 844 (2020), Article 156034, 10.1016/j.jallcom.2020.156034 ↗

 [View PDF](#) [View article](#) [View in Scopus ↗](#) [Google Scholar ↗](#)

- [23] P. Yue, Z. Wang, W. Peng, L. Li, H. Guo, X. Li, Q. Hu, Y. Zhang
Preparation and electrochemical properties of submicron LiNi 0.6Co0.2Mn0.2O2 as cathode material for lithium ion batteries

Scr Mater, 65 (2011), pp. 1077-1080, 10.1016/j.scriptamat.2011.09.020 ↗

 [View PDF](#) [View article](#) [View in Scopus ↗](#) [Google Scholar ↗](#)

- [24] Y. Zheng, R. Zhang, P. Vanaphuti, Y. Liu, Z. Yang, Y. Wang
Positive role of fluorine impurity in recovered LiNi0.6Co0.2Mn0.2O2Cathode materials

ACS Appl. Mater. Interfaces, 13 (2021), pp. 57171-57181, 10.1021/acsami.1c17341 ↗

[View in Scopus ↗](#) [Google Scholar ↗](#)

- [25] B. Wu, J. Bi, Q. Liu, D. Mu, L. Wang, J. Fu, F. Wu
Role of current density in the degradation of LiNi 0.6 Co 0.2 Mn 0.2 O 2 cathode material





Electrochim. Acta, 298 (2019), pp. 609-615, 10.1016/j.electacta.2018.12.127 ↗

 [View PDF](#) [View article](#) [View in Scopus ↗](#) [Google Scholar ↗](#)

- [26] W. Ahn, S.N. Lim, K.N. Jung, S.H. Yeon, K.B. Kim, H.S. Song, K.H. Shin
Combustion-synthesized LiNi0.6Mn0.2Co 0.2O2 as cathode material for lithium ion batteries

J. Alloys Compd., 609 (2014), pp. 143-149, 10.1016/j.jallcom.2014.03.123 ↗

 [View PDF](#) [View article](#) [View in Scopus](#) [Google Scholar](#)

- [27] H. Lu, H. Zhou, A.M. Svensson, A. Fossdal, E. Sheridan, S. Lu, F. Vullum-Bruer
High capacity Li[Ni_{0.8}Co_{0.1}Mn_{0.1}]O₂ synthesized by sol-gel and co-precipitation methods as cathode materials for lithium-ion batteries
Solid State Ion (2013), pp. 249-250, 10.1016/j.ssi.2013.07.023 [View in Scopus](#)
105–111
[Google Scholar](#)
- [28] J. Li, M. Zhang, D. Zhang, Y. Yan, Z. Li, Z. Nie
Effect of sintering conditions on electrochemical properties of LiNi_{0.8}Co_{0.1}Mn_{0.1}O₂ as cathode material
Int. J. Electrochem. Sci., 15 (2020), pp. 1881-1892, 10.20964/2020.03.63 [View in Scopus](#)
 [View PDF](#) [View article](#) [View in Scopus](#) [Google Scholar](#)
- [29] Y. Xi, Y. Liu, D. Zhang, S. Jin, R. Zhang, M. Jin
Comparative study of the electrochemical performance of LiNi_{0.5}Co_{0.2}Mn_{0.3}O₂ and LiNi_{0.8}Co_{0.1}Mn_{0.1}O₂ cathode materials for lithium ion batteries
Solid State Ion, 327 (2018), pp. 27-31, 10.1016/j.ssi.2018.10.020 [View in Scopus](#)
 [View PDF](#) [View article](#) [View in Scopus](#) [Google Scholar](#)
- [30] Y. Zhang, K. Du, Y. Cao, Y. Lu, Z. Peng, J. Fan, L. Li, Z. Xue, H. Su, G. Hu
Hydrothermal preparing agglomerate LiNi_{0.8}Co_{0.1}Mn_{0.1}O₂ cathode material with submicron primary particle for alleviating microcracks
J. Power Sources, 477 (2020), Article 228701, 10.1016/j.jpowsour.2020.228701 [View in Scopus](#)
 [View PDF](#) [View article](#) [View in Scopus](#) [Google Scholar](#)
- [31] M. Shang, X. Chen, J. Niu
Nickel-rich layered LiNi_{0.8}Mn_{0.1}Co_{0.1}O₂ with dual gradients on both primary and secondary particles in lithium-ion batteries
Cell Rep Phys Sci, 3 (2022), Article 100767, 10.1016/j.xcrp.2022.100767 [View in Scopus](#)
 [View PDF](#) [View article](#) [View in Scopus](#) [Google Scholar](#)
- [32] H. Darjazi, E. Gonzalo, B. Acebedo, R. Cid, M. Zarrabeitia, F. Bonilla, M.Á. Muñoz-Márquez, F. Nobili
Improving high-voltage cycling performance of nickel-rich NMC layered oxide cathodes for rechargeable lithium-ion batteries by Mg and Zr co-

doping

Materials Today Sustainability, 20 (2022), Article 100236, 10.1016/j.mtsust.2022.100236 ↗

 View PDF View article View in Scopus ↗ Google Scholar ↗

[33] Y. Gao, J. Park, X. Liang

Comprehensive study of Al- and Zr-modified $\text{LiNi}_{0.8}\text{Mn}_{0.1}\text{Co}_{0.1}\text{O}_2$ through synergy of coating and doping

ACS Appl. Energy Mater., 3 (2020), pp. 8978-8987, 10.1021/acsaem.0c01420 ↗

View in Scopus ↗ Google Scholar ↗

[34] F. Xin, H. Zhou, X. Chen, M. Zuba, N. Chernova, G. Zhou, M.S. Whittingham, -O. Li-Nb

Coating/Substitution enhances the electrochemical performance of the $\text{LiNi}_{0.8}\text{Mn}_{0.1}\text{Co}_{0.1}\text{O}_2$ (NMC 811) cathode

ACS Appl. Mater. Interfaces, 11 (2019), pp. 34889-34894, 10.1021/acsami.9b09696 ↗

View in Scopus ↗ Google Scholar ↗

[35] C.Y. Wu, Q. Bao, Y.T. Tsai, J.G. Duh

Tuning (003) interplanar space by boric acid co-sintering to enhance Li^+ storage and transfer in $\text{Li}(\text{Ni}_{0.8}\text{Co}_{0.1}\text{Mn}_{0.1})\text{O}_2$ cathode

J. Alloys Compd., 865 (2021), Article 158806, 10.1016/j.jallcom.2021.158806 ↗

 View PDF View article View in Scopus ↗ Google Scholar ↗

[36] L. Azhari, B. Sousa, R. Ahmed, R. Wang, Z. Yang, G. Gao, Y. Han, Y. Wang

Stability enhancement and microstructural modification of Ni-rich cathodes via halide doping

ACS Appl. Mater. Interfaces, 14 (2022), pp. 46523-46536, 10.1021/acsami.2c11773 ↗

View in Scopus ↗ Google Scholar ↗

[37] H. Sun, K. Zhao

Electronic structure and comparative properties of $\text{LiNi}_x\text{Mn}_y\text{Co}_z\text{O}_2$ cathode materials

J. Phys. Chem. C, 121 (2017), pp. 6002-6010, 10.1021/acs.jpcc.7b00810 ↗





Google Scholar ↗

[38] X.-G. Sun, C.J. Jafta, S. Tan, A. Borisevich, R.B. Gupta, M.P. Paranthaman

Facile surface coatings for performance improvement of NMC811 battery cathode material

J. Electrochem. Soc., 169 (2022), Article 020565, 10.1149/1945-7111/ac5302 ↗

[View in Scopus ↗](#) [Google Scholar ↗](#)

- [39] Y. Wu, M. Li, W. Wahyudi, G. Sheng, X. Miao, T.D. Anthopoulos, K.W. Huang, Y. Li, Z. Lai
Performance and stability improvement of layered NCM lithium-ion
batteries at high voltage by a microporous Al₂O₃ sol-gel coating
ACS Omega, 4 (2019), pp. 13972-13980, 10.1021/acsomega.9b01706 [↗](#)
[View in Scopus ↗](#) [Google Scholar ↗](#)
- [40] S. Liu, Z. Dang, D. Liu, C. Zhang, T. Huang, A. Yu
Comparative studies of zirconium doping and coating on
LiNi_{0.6}Co_{0.2}Mn_{0.2}O₂ cathode material at elevated temperatures
J. Power Sources, 396 (2018), pp. 288-296, 10.1016/j.jpowsour.2018.06.052 [↗](#)
 [View PDF](#) [View article](#) [View in Scopus ↗](#) [Google Scholar ↗](#)
- [41] J.H. Shim, Y.M. Kim, M. Park, J. Kim, S. Lee
Reduced graphene oxide-wrapped nickel-rich cathode materials for lithium
ion batteries
ACS Appl. Mater. Interfaces, 9 (2017), pp. 18720-18729, 10.1021/acsami.7b02654 [↗](#)
[View in Scopus ↗](#) [Google Scholar ↗](#)
- [42] S.J. Do, P. Santhoshkumar, S.H. Kang, K. Prasanna, Y.N. Jo, C.W. Lee
Al-doped Li[Ni_{0.78}Co_{0.1}Mn_{0.1}Al_{0.02}]O₂ for high performance of
lithium ion batteries
Ceram. Int., 45 (2019), pp. 6972-6977, 10.1016/j.ceramint.2018.12.196 [↗](#)
 [View PDF](#) [View article](#) [View in Scopus ↗](#) [Google Scholar ↗](#)
- [43] G. Zha, W. Hu, S. Agarwal, C. Ouyang, N. Hu, H. Hou
High performance layered LiNi_{0.8}Co_{0.07}Fe_{0.03}Mn_{0.1}O₂ cathode materials
for Li-ion battery
Chem. Eng. J., 409 (2021), Article 128343, 10.1016/j.cej.2020.128343 [↗](#)
 [View PDF](#) [View article](#) [View in Scopus ↗](#) [Google Scholar ↗](#)
- [44] H. Yuan, W. Song, M. Wang, Y. Gu, Y. Chen
Lithium-ion conductive coating layer on nickel rich layered oxide cathode
material with improved electrochemical properties for Li-ion battery
J. Alloys Compd., 784 (2019), pp. 1311-1322, 10.1016/j.jallcom.2019.01.072 [↗](#)
 [View PDF](#) [View article](#) [View in Scopus ↗](#) [Google Scholar ↗](#)
- [45] H. Khalid, A.A. Chaudhry

4 - basics of hydroxyapatite—structure, synthesis, properties, and clinical applications

A.S. Khan, A.A. Chaudhry (Eds.), Handbook of Ionic Substituted Hydroxyapatites, Woodhead Publishing (2020), pp. 85-115, 10.1016/B978-0-08-102834-6.00004-5 ↗

 [View PDF](#) [View article](#) [View in Scopus](#) ↗ [Google Scholar](#) ↗

- [46] D. Wang, I. Belharouak, G.M. Koenig, G. Zhou, K. Amine
Growth mechanism of $\text{Ni}_{0.3}\text{Mn}_{0.7}\text{CO}_3$ precursor for high capacity Li-ion battery cathodes

J. Mater. Chem., 21 (2011), pp. 9290-9295, 10.1039/C1JM11077B ↗

[View in Scopus](#) ↗ [Google Scholar](#) ↗

- [47] L. Liang, K. Du, Z. Peng, Y. Cao, J. Duan, J. Jiang, G. Hu
Co-precipitation synthesis of $\text{Ni}_{0.6}\text{Co}_{0.2}\text{Mn}_{0.2}(\text{OH})_2$ precursor and characterization of $\text{LiNi}_{0.6}\text{Co}_{0.2}\text{Mn}_{0.2}\text{O}_2$ cathode material for secondary lithium batteries

Electrochim. Acta, 130 (2014), pp. 82-89, 10.1016/j.electacta.2014.02.100 ↗

 [View PDF](#) [View article](#) [View in Scopus](#) ↗ [Google Scholar](#) ↗

- [48] F. Zhou, X. Zhao, A. van Bommel, A.W. Rowe, J.R. Dahn
Coprecipitation synthesis of $\text{Ni}_x\text{Mn}_{1-x}(\text{OH})_2$ mixed hydroxides

Chem. Mater., 22 (2010), pp. 1015-1021, 10.1021/cm9018309 ↗

[View in Scopus](#) ↗ [Google Scholar](#) ↗

- [49] D.-L. Vu, J. Lee
Properties of $\text{LiNi}_{0.8}\text{Co}_{0.1}\text{Mn}_{0.1}\text{O}_2$ as a high energy cathode material for lithium-ion batteries

Kor. J. Chem. Eng., 33 (2016), pp. 514-526, 10.1007/s11814-015-0154-3 ↗

[View in Scopus](#) ↗ [Google Scholar](#) ↗

- [50] D.S. Hall, D.J. Lockwood, C. Bock, B.R. MacDougall
Nickel hydroxides and related materials: a review of their structures, synthesis and properties

Proc. R. Soc. A, 471 (2015), 10.1098/rspa.2014.0792 ↗

[Google Scholar](#) ↗

- [51] L. Xu, F. Zhou, J. Kong, H. Zhou, Q. Zhang, Q. Wang, G. Yan

Influence of precursor phase on the structure and electrochemical properties of $\text{Li}(\text{Ni}_{0.6}\text{Mn}_{0.2}\text{Co}_{0.2})\text{O}_2$ cathode materials

Solid State Ion, 324 (2018), pp. 49-58, 10.1016/j.ssi.2018.06.010 ↗

 View PDF View article View in Scopus ↗ Google Scholar ↗

- [52] S. Zhang, C. Deng, B.L. Fu, S.Y. Yang, L. Ma
Synthetic optimization of spherical $\text{Li}[\text{Ni}_{1/3}\text{Mn}_{1/3}\text{Co}_{1/3}]\text{O}_2$ prepared by a carbonate co-precipitation method

Powder Technol., 198 (2010), pp. 373-380, 10.1016/j.powtec.2009.12.002 ↗

 View PDF View article View in Scopus ↗ Google Scholar ↗

- [53] Q. Zhu, H. Xiao, R. Zhang, S. Geng, Q. Huang
Effect of impeller type on preparing spherical and dense $\text{Ni}_{1-x-y}\text{Co}_x\text{Mn}_y(\text{OH})_2$ precursor via continuous co-precipitation in pilot scale: a case of $\text{Ni}_{0.6}\text{Co}_{0.2}\text{Mn}_{0.2}(\text{OH})_2$

Electrochim. Acta, 318 (2019), pp. 1-13, 10.1016/j.electacta.2019.06.008 ↗

 View PDF View article View in Scopus ↗ Google Scholar ↗

- [54] B.C. Alpay, O. Keles
Effect of impeller design on the properties of $\text{Li}_{1.03}\text{Ni}_{0.8}\text{Mn}_{0.1}\text{Co}_{0.1}\text{O}_2$ cathode material synthesized via co-precipitation method

J. Alloys Compd., 947 (2023), Article 169583, 10.1016/j.jallcom.2023.169583 ↗

 View PDF View article View in Scopus ↗ Google Scholar ↗

- [55] J. Zheng, P. Yan, L. Estevez, C. Wang, J.-G. Zhang
Effect of calcination temperature on the electrochemical properties of nickel-rich $\text{LiNi}_{0.76}\text{Mn}_{0.14}\text{Co}_{0.1}\text{O}_2$ cathodes for lithium-ion batteries

Nano Energy, 49 (2018), pp. 538-548, 10.1016/j.nanoen.2018.04.077 ↗

 View PDF View article View in Scopus ↗ Google Scholar ↗

- [56] H.N. Pollen, J.R. Tolchard, A.M. Svensson, N.P. Wagner
A single-pot Co-precipitation synthesis route for Ni-rich layered oxide materials with high cycling stability

Chemelectrochem, 9 (2022), 10.1002/celc.202200859 ↗

Google Scholar ↗

- [57] B. Zhu, Z. Xu, Y. Ning, G. Wei, J. Qu

Managing ammonia-alkali balance to control precursor characteristics in co-precipitation process for enhanced electrochemical performance of nickel-rich cathode materials

Solid State Sci., 142 (2023), Article 107224, 10.1016/j.solidstatesciences.2023.107224 ↗

 View PDF View article View in Scopus ↗ Google Scholar ↗

- [58] J. Duan, R. Zhang, Q. Zhu, H. Xiao, Q. Huang

The effect of controlling strategies of pH and ammonia concentration on preparing full concentration gradient $\text{Ni}_{0.8}\text{Co}_{0.1}\text{Mn}_{0.1}(\text{OH})_2$ via coprecipitation in a pilot-scale reactor

Energy Technol., 8 (2020), Article 1901437, 10.1002/ente.201901437 ↗

View in Scopus ↗ Google Scholar ↗

- [59] F. Bizzotto, W. Dachraoui, R. Grissa, W. Zhao, F. Pagani, E. Querel, R.-S. Kühnel, C. Battaglia
Modification of NMC811 with titanium for enhanced cycling and high-voltage stability

Electrochim. Acta, 462 (2023), Article 142758, 10.1016/j.electacta.2023.142758 ↗

 View PDF View article View in Scopus ↗ Google Scholar ↗

- [60] M.M.S. Sanad, N.K. Meselhy, H.A. El-Boraey, A. Toghan
Controllable engineering of new ZnAl_2O_4 -decorated $\text{LiNi}_{0.8}\text{Mn}_{0.1}\text{Co}_{0.1}\text{O}_2$ cathode materials for high performance lithium-ion batteries

J. Mater. Res. Technol., 23 (2023), pp. 1528-1542, 10.1016/j.jmrt.2023.01.102 ↗

 View PDF View article View in Scopus ↗ Google Scholar ↗

- [61] A. Gomez-Martin, F. Reissig, L. Frankenstein, M. Heidbüchel, M. Winter, T. Placke, R. Schmuch
Magnesium substitution in Ni-rich NMC layered cathodes for high-energy lithium ion batteries

Adv. Energy Mater., 12 (2022), Article 2103045, 10.1002/aenm.202103045 ↗

View in Scopus ↗ Google Scholar ↗

- [62] C. Savaş Uygur, M.K. Aydınol
Effect of calcium or yttrium doping on cation ordering and electrochemical performance of $\text{Li}(\text{Ni}_{0.80-x}\text{Co}_{0.15}\text{Al}_{0.05}\text{M}_x)\text{O}_2$ (M = Ca, Y) as a Li-ion battery cathode

Mater. Sci. Eng., B, 264 (2021), Article 114925, 10.1016/j.mseb.2020.114925 ↗

 View PDF View article View in Scopus ↗ Google Scholar ↗

- [63] M.M.S. Sanad, N.K. Meselhy, H.A. El-Boraey
Surface protection of NMC811 cathode material via ZnSnO₃ perovskite film for enhanced electrochemical performance in rechargeable Li-ion batteries
Colloids Surf. A Physicochem. Eng. Asp., 672 (2023), Article 131748,
 10.1016/j.colsurfa.2023.131748 [↗](#)
[View PDF](#) [View article](#) [View in Scopus](#) [Google Scholar](#) [↗](#)
- [64] W.H. Low, P.S. Khiew, S.S. Lim, C.W. Siong, E.R. Ezeigwe
Recent development of mixed transition metal oxide and graphene/mixed transition metal oxide based hybrid nanostructures for advanced supercapacitors
J. Alloys Compd., 775 (2019), pp. 1324-1356, 10.1016/j.jallcom.2018.10.102 [↗](#)
[View PDF](#) [View article](#) [View in Scopus](#) [Google Scholar](#) [↗](#)
- [65] A.E. Danks, S.R. Hall, Z. Schnepf
The evolution of “sol-gel” chemistry as a technique for materials synthesis
Mater. Horiz., 3 (2016), pp. 91-112, 10.1039/c5mh00260e [↗](#)
[View in Scopus](#) [Google Scholar](#) [↗](#)
- [66] L. Chen, W. Feng, Z. Pu, X. Wang, C. Song
Impact of pH on preparation of LiFePO₄@C cathode materials by a sol-gel route assisted by biomineralization
Ionics, 25 (2019), pp. 5625-5632, 10.1007/s11581-019-03273-1 [↗](#)
[View in Scopus](#) [Google Scholar](#) [↗](#)
- [67] C. Huck-Iriart, N.J. Morales, M.L. Herrera, R.J. Candal
Micro to mesoporous SiO₂xerogels: the effect of acid catalyst type in sol-gel process
J. Sol. Gel Sci. Technol., 102 (2022), pp. 197-207, 10.1007/s10971-021-05601-2 [↗](#)
[View in Scopus](#) [Google Scholar](#) [↗](#)
- [68] B. You, Z. Wang, F. Shen, Y. Chang, W. Peng, X. Li, H. Guo, Q. Hu, C. Deng, S. Yang, G. Yan, J. Wang
Research progress of single-crystal nickel-rich cathode materials for lithium ion batteries
Small Methods, 5 (2021), Article 2100234, 10.1002/smt.202100234 [↗](#)
[View in Scopus](#) [Google Scholar](#) [↗](#)

- [69] H. Liu, Y.P. Wu, E. Rahm, R. Holze, H.Q. Wu
Cathode materials for lithium ion batteries prepared by sol-gel methods
J. Solid State Electrochem., 8 (2004), pp. 450-466, 10.1007/s10008-004-0521-1 [↗](#)
[Google Scholar ↗](#)
- [70] J.D. Mackenzie
Applications of the sol-gel process
J. Non-Cryst. Solids, 100 (1988), pp. 162-168, 10.1016/0022-3093(88)90013-0 [↗](#)
[View PDF](#) [View article](#) [View in Scopus ↗](#) [Google Scholar ↗](#)
- [71] C. Song, W. Feng, W. Su, L. Chen, M. Li
Effect of drying time on electrochemical properties of Li_{1.2}Mn_{0.54}Ni_{0.13}Co_{0.13}O₂ cathode material
Int. J. Electrochem. Sci., 14 (2019), pp. 2372-2382, 10.20964/2019.03.20 [↗](#)
[View PDF](#) [View article](#) [View in Scopus ↗](#) [Google Scholar ↗](#)
- [72] C. Song, W. Feng, Z. Shi, X. Wang
Effect of drying temperature on properties of lithium-rich manganese-based materials in sol-gel method
Ionics, 25 (2019), pp. 4607-4614, 10.1007/s11581-019-03012-6 [↗](#)
[View in Scopus ↗](#) [Google Scholar ↗](#)
- [73] J. Ungula, B.F. Dejene
Effect of solvent medium on the structural, morphological and optical properties of ZnO nanoparticles synthesized by the sol-gel method
Physica B Condens Matter, 480 (2016), pp. 26-30, 10.1016/j.physb.2015.10.007 [↗](#)
[View PDF](#) [View article](#) [View in Scopus ↗](#) [Google Scholar ↗](#)
- [74] F. Oksuzomer, S.N. Koc, I. Boz, M.A. Gurkaynak
Effect of solvents on the preparation of lithium aluminate by sol-gel method
Mater. Res. Bull., 39 (2004), pp. 715-724, 10.1016/j.materresbull.2003.10.022 [↗](#)
[View PDF](#) [View article](#) [View in Scopus ↗](#) [Google Scholar ↗](#)
- [75] W. Li, L. Yao, X. Zhang, W. Lang, J. Si, J. Yang, L. Li
The effect of chelating agent on synthesis and electrochemical properties of LiNi_{0.6}Co_{0.2}Mn_{0.2}O₂
SN Appl. Sci., 2 (2020), p. 554, 10.1007/s42452-020-2377-0 [↗](#)

[View in Scopus](#) [Google Scholar](#)

[76] M.A. Fardad

Catalysts and the structure of SiO₂ sol-gel films

J. Mater. Sci., 35 (2000), pp. 1835-1841, 10.1023/A:1004749107134

[View in Scopus](#) [Google Scholar](#)

[77] N. Kızıltaş-Yavuz, M. Herklotz, A.M. Hashem, H.M. Abuzeid, B. Schwarz, H. Ehrenberg, A. Mauger, C.M. Julien

Synthesis, structural, magnetic and electrochemical properties of LiNi_{1/3}Mn_{1/3}Co_{1/3}O₂ prepared by a sol-gel method using table sugar as chelating agent

Electrochim. Acta, 113 (2013), pp. 313-321, 10.1016/j.electacta.2013.09.065

 [View PDF](#) [View article](#) [View in Scopus](#) [Google Scholar](#)

[78] G. Singh, A. Sil, S. Ghosh, A. Panwar

Effect of citric acid content on synthesis of LiNi_{1/3}Mn_{1/3}Co_{1/3}O₂ and its electrochemical characteristics

Ceram. Int., 36 (2010), pp. 1831-1836, 10.1016/j.ceramint.2010.03.028

 [View PDF](#) [View article](#) [View in Scopus](#) [Google Scholar](#)

[79] Z. Liu, L. Li, J. Chen, H. Yang, L. Xia, J. Chen, J. Duan, Z. Chen

Effects of chelating agents on electrochemical properties of Na_{0.9}Ni_{0.45}Mn_{0.55}O₂ cathode materials

J. Alloys Compd., 855 (2021), Article 157485, 10.1016/j.jallcom.2020.157485

 [View PDF](#) [View article](#) [View in Scopus](#) [Google Scholar](#)

[80] O. Sha, S. Wang, Z. Qiao, W. Yuan, Z. Tang, Q. Xu, Y. Su

Synthesis of spinel LiNi_{0.5}Mn_{1.5}O₄ cathode material with excellent cycle stability using urea-based sol-gel method





Mater. Lett., 89 (2012), pp. 251-253, 10.1016/j.matlet.2012.08.126

 [View PDF](#) [View article](#) [View in Scopus](#) [Google Scholar](#)

[81] Q. Wu, L. Zhao, J. Wu

Effects of chelating agents on the performance of Li_{1.2}Mn_{0.54}Ni_{0.13}Co_{0.13}O₂ as cathode material for Li-ion battery prepared by sol-gel method

J. Sol. Gel Sci. Technol., 82 (2017), pp. 335-343, 10.1007/s10971-017-4338-7

- [82] S.S. Alias, A.B. Ismail, A.A. Mohamad
 Effect of pH on ZnO nanoparticle properties synthesized by sol–gel centrifugation
 J. Alloys Compd., 499 (2010), pp. 231-237, 10.1016/j.jallcom.2010.03.174 ↗
 View PDF View article View in Scopus ↗ Google Scholar ↗
- [83] J. Zhang, J. Zheng, Y. Li, Y. Liu, W. Hao, L. Lin, Y. Li, J. Song
 Effect of different pH values adjusted by ammonia on the dielectric properties of CaCu₃Ti₄O₁₂ ceramics prepared by a sol-gel method
 J. Alloys Compd., 779 (2019), pp. 255-260, 10.1016/j.jallcom.2018.11.244 ↗
 View PDF View article Google Scholar ↗
- [84] J. Du, Z. Liu, Z. Zhu
 In situ characterization of Ni-rich NMC811 thin films prepared by sol-gel method using different scanning probe microscopy techniques
 Ceram. Int., 49 (2023), pp. 31485-31495, 10.1016/j.ceramint.2023.07.096 ↗
 View PDF View article View in Scopus ↗ Google Scholar ↗
- [85] D. Jiang, L. Zhao, Y. Shao, D. Wang
 Preparation and characterization of layered LiNi_{0.9}Co_{0.05}Mn_{0.025}Mg_{0.025}O₂ cathode material by a sol-gel method for lithium-ion batteries
 RSC Adv., 5 (2015), pp. 40779-40784, 10.1039/c5ra05669a ↗
 View in Scopus ↗ Google Scholar ↗
- [86] S.W. Lee, H. Kim, M.S. Kim, H.C. Youn, K. Kang, B.W. Cho, K.C. Roh, K.B. Kim
 Improved electrochemical performance of LiNi_{0.6}Co_{0.2}Mn_{0.2}O₂ cathode material synthesized by citric acid assisted sol-gel method for lithium ion batteries
 J. Power Sources, 315 (2016), pp. 261-268, 10.1016/j.jpowsour.2016.03.020 ↗
 View PDF View article View in Scopus ↗ Google Scholar ↗
- [87] H. Lu, H. Zhou, A.M. Svensson, A. Fossdal, E. Sheridan, S. Lu, F. Vullum-Bruer
 High capacity Li[Ni_{0.8}Co_{0.1}Mn_{0.1}]O₂ synthesized by sol–gel and co-precipitation methods as cathode materials for lithium-ion batteries
 Solid State Ion (2013), pp. 249-250, 10.1016/j.ssi.2013.07.023 ↗

Google Scholar ↗

[88] R. Santhanam, B. Rambabu

High rate cycling performance of $\text{Li}_{1.05}\text{Ni}_{1/3}\text{Co}_{1/3}\text{Mn}_{1/3}\text{O}_2$ materials prepared by sol-gel and co-precipitation methods for lithium-ion batteries

J. Power Sources, 195 (2010), pp. 4313-4317, 10.1016/j.jpowsour.2010.01.016 ↗

 View PDF View article View in Scopus ↗ Google Scholar ↗

[89] S. Engün, K.B. Dermenci, U. Savacı, C.C. Erdoğan, S. Turan

Unveiling the Enhanced Electrochemical Performance of $\text{LiNi}_{0.5}\text{Mn}_{0.3}\text{Co}_{0.2}\text{O}_2$ sol-gel coated with Li-La-Zr-O based gel

J. Alloys Compd., 957 (2023), 10.1016/j.jallcom.2023.170466 ↗

Google Scholar ↗

[90] R. Li, S. Zeng, K. Shen, G. Wang, J. Zhang

Effects of mechanical grinding on the physicochemical properties of silica aerogels

Front Mater, 10 (2023), 10.3389/fmats.2023.1225481 ↗

Google Scholar ↗

[91] W. Hao, H. Zhan, H. Chen, Y. Wang, Q. Tan, F. Su

Solid-state synthesis of $\text{Li}[\text{Li}_{0.2}\text{Mn}_{0.56}\text{Ni}_{0.16}\text{Co}_{0.08}]\text{O}_2$ cathode materials for lithium-ion batteries

Particuology, 15 (2014), pp. 18-26, 10.1016/j.partic.2013.01.004 ↗

 View PDF View article View in Scopus ↗ Google Scholar ↗

[92] C. Zhao, Q. Shen

Organic acid assisted solid-state synthesis of $\text{Li}_{1.2}\text{Ni}_{0.16}\text{Co}_{0.08}\text{Mn}_{0.56}\text{O}_2$ nanoparticles as lithium ion battery cathodes

Curr. Appl. Phys., 14 (2014), pp. 1849-1853, 10.1016/j.cap.2014.10.020 ↗

 View PDF View article View in Scopus ↗ Google Scholar ↗

[93] J. Karunawan, O. Floweri, S.P. Santosa, A. Sumboja, F. Iskandar

Stable layered-layered-spinel structure of the $\text{Li}_{1.2}\text{Ni}_{0.13}\text{Co}_{0.13}\text{Mn}_{0.54}\text{O}_2$ cathode synthesized by ball-milling assisted solid-state method

J. Electroanal. Chem., 907 (2022), 10.1016/j.jelechem.2022.116050 ↗

Google Scholar ↗

[94] X. Jiang, Y. Sha, R. Cai, Z. Shao

The solid-state chelation synthesis of $\text{LiNi}_{1/3}\text{Co}_{1/3}\text{Mn}_{1/3}\text{O}_2$ as a cathode material for lithium-ion batteries

J Mater Chem A Mater, 3 (2015), pp. 10536-10544, 10.1039/c5ta01236h ↗

View in Scopus ↗ Google Scholar ↗

[95] C. Suryanarayana

Mechanical alloying and milling

Prog. Mater. Sci., 46 (2001), pp. 1-184, 10.1016/S0079-6425(99)00010-9 ↗

 View PDF View article View in Scopus ↗ Google Scholar ↗

[96] R. Brow, A. Donakowski, A. Mesnier, D.J. Pereira, K.X. Steirer, S. Santhanagopalan, A. Manthiram

Mechanical pulverization of Co-free nickel-rich cathodes for improved high-voltage cycling of lithium-ion batteries

ACS Appl. Energy Mater., 5 (2022), pp. 6996-7005, 10.1021/acsaem.2c00606 ↗

View in Scopus ↗ Google Scholar ↗

[97] A. Tron, M. Hong, Y. Don Park, J. Kim, J. Mun

Ni-rich layered cathode materials by a mechanochemical method for high-energy lithium-ion batteries

ChemistrySelect, 5 (2020), pp. 14596-14601, 10.1002/slct.202003884 ↗

View in Scopus ↗ Google Scholar ↗

[98] H. He, J. Dong, D. Zhang, D. Hang, X. Zhu, C. Chang

Feasible synthesis of NCM811 cathodes with controllable Li/Ni cationic mixing for enhanced electrochemical performance via a nano grinding assisted solid-state approach

Int. J. Energy Res., 45 (2021), pp. 7108-7119, 10.1002/er.6296 ↗

View in Scopus ↗ Google Scholar ↗


[99] Mintarsih Rahmawati, Agus Purwanto, Hendri Widiyandari, Tika Paramitha, Muhammad Nizam, Endah Retno Dyartanti, Soraya Ulfa Muzayahna, Yudha Cornelius Satria

Synthesis of NMC 111 via urea assisted solid state method

AIP Conf. Proc., 2197 (2020), Article 050007

<https://pubs.aip.org/aip/acp/article-abstract/2197/1/050007/782662/Synthesis-of-NMC-111-via-urea-assisted-solid-state> ↗, Accessed 17th Aug 2023

[CrossRef ↗](#) [View in Scopus ↗](#) [Google Scholar ↗](#)

- [100] C. Liu, M. Wu, Y. Liu, Z. Lu, Y. Yang, S. Shi, G. Yang
Effect of ball milling conditions on microstructure and lithium storage properties of $\text{LiNi}_{0.5}\text{Mn}_{1.5}\text{O}_4$ as cathode for lithium-ion batteries
Mater. Res. Bull., 99 (2018), pp. 436-443, 10.1016/j.materresbull.2017.11.048 [↗](#)
 [View PDF](#) [View article](#) [View in Scopus ↗](#) [Google Scholar ↗](#)
- [101] K. Yuan, T. Tu, C. Shen, L. Zhou, J. Liu, J. Li, K. Xie, G. Zhang
Self-ball milling strategy to construct high-entropy oxide coated $\text{LiNi}_{0.8}\text{Co}_{0.1}\text{Mn}_{0.1}\text{O}_2$ with enhanced electrochemical performance
Journal of Advanced Ceramics, 11 (2022), pp. 882-892, 10.1007/s40145-022-0582-6 [↗](#)
[View in Scopus ↗](#) [Google Scholar ↗](#)
- [102] L. Li, L. Xia, H. Yang, X. Zhan, J. Chen, Z. Chen, J. Duan
Solid-state synthesis of lanthanum-based oxides Co-coated $\text{LiNi}_{0.5}\text{Co}_{0.2}\text{Mn}_{0.3}\text{O}_2$ for advanced lithium ion batteries
J. Alloys Compd., 832 (2020), 10.1016/j.jallcom.2020.154959 [↗](#)
[Google Scholar ↗](#)
- [103] T. Pan, J. Alvarado, J. Zhu, Y. Yue, H.L. Xin, D. Nordlund, F. Lin, M.M. Doeff
Structural degradation of layered cathode materials in lithium-ion batteries induced by ball milling
J. Electrochem. Soc., 166 (2019), pp. A1964-A1971, 10.1149/2.0091910jes [↗](#)
[View in Scopus ↗](#) [Google Scholar ↗](#)
- [104] M. Stein, C.F. Chen, M. Mullings, D. Jaime, A. Zaleski, P.P. Mukherjee, C.P. Rhodes
Probing the effect of high energy ball milling on the structure and properties of $\text{LiNi}_{1/3}\text{Mn}_{1/3}\text{Co}_{1/3}\text{O}_2$ cathodes for Li-ion batteries
Journal of Electrochemical Energy Conversion and Storage (2016), p. 13, 10.1115/1.4034755 [↗](#)
[View in Scopus ↗](#) [Google Scholar ↗](#)
- [105] D. Vernardou
Recent report on the hydrothermal growth of LiFePO_4 as a cathode material
Coatings, 12 (2022), 10.3390/coatings12101543 [↗](#)
[Google Scholar ↗](#)
- [106] Y. Han, Y. Lei, J. Ni, Y. Zhang, Z. Geng, P. Ming, C. Zhang, X. Tian, J.L. Shi, Y.G. Guo, Q. Xiao

Single-crystalline cathodes for advanced Li-ion batteries: progress and challenges

Small, 18 (2022), 10.1002/sml.202107048 ↗

Google Scholar ↗

[107] G.B. Nair, H.C. Swart, S.J. Dhoble

A review on the advancements in phosphor-converted light emitting diodes (pc-LEDs): phosphor synthesis, device fabrication and characterization

Prog. Mater. Sci., 109 (2020), Article 100622, 10.1016/j.pmatsci.2019.100622 ↗

 View PDF View article View in Scopus ↗ Google Scholar ↗

[108] A. V Nikam, B.L. V Prasad, A.A. Kulkarni

Wet chemical synthesis of metal oxide nanoparticles: a review

CrystEngComm, 20 (2018), pp. 5091-5107, 10.1039/C8CE00487K ↗

Google Scholar ↗

[109] Y. Shi, M. Zhang, C. Fang, Y.S. Meng

Urea-based hydrothermal synthesis of $\text{LiNi}_{0.5}\text{Co}_{0.2}\text{Mn}_{0.3}\text{O}_2$ cathode material for Li-ion battery

J. Power Sources, 394 (2018), pp. 114-121, 10.1016/j.jpowsour.2018.05.030 ↗

 View PDF View article View in Scopus ↗ Google Scholar ↗

[110] J. Li, W. Zhong, Q. Deng, Q. Zhang, C. Yang

Recent progress in synthesis and surface modification of nickel-rich layered oxide cathode materials for lithium-ion batteries

Int. J. Extrem. Manuf., 4 (2022), 10.1088/2631-7990/ac92ef ↗

Google Scholar ↗

[111] J. Liu, W. Jiao, X. Wang, G. Mao, Y. Yao, W. Yu, H. Tong

Uniformly sodium ions doped $\text{LiNi}_{0.84}\text{Co}_{0.11}\text{Mn}_{0.05}\text{O}_2$ cathode material with high performance for lithium-ion batteries

Ceram. Int., 49 (2023), pp. 13953-13959, 10.1016/j.ceramint.2022.12.277 ↗

 View PDF View article View in Scopus ↗ Google Scholar ↗

[112] J. Langdon, A. Manthiram

A perspective on single-crystal layered oxide cathodes for lithium-ion batteries

Energy Storage Mater., 37 (2021), pp. 143-160, 10.1016/j.ensm.2021.02.003 ↗

 [View PDF](#) [View article](#) [View in Scopus](#)  [Google Scholar](#) 

- [113] V. Mathew, B. Sambandam, S. Kim, S. Kim, S. Park, S. Lee, J. Lee, S. Park, J. Song, J. Kim
High-voltage cathode materials by combustion-based preparative approaches for Li-ion batteries application

J. Power Sources, 472 (2020), Article 228368, 10.1016/j.jpowsour.2020.228368 


 [View PDF](#) [View article](#) [View in Scopus](#)  [Google Scholar](#) 

- [114] S.O. Ajayi, C.O. Ehi-Eromosele, K.O. Ajanaku
Combustion synthesis and characterization of $\text{Li}_{1.2}\text{Mn}_{0.52}\text{Ni}_{0.20}\text{Co}_{0.08}\text{O}_2$ cathodes for Li-Ion battery: effect of fuel mixture and annealing temperature

Ceram. Int., 48 (2022), pp. 2306-2316, 10.1016/j.ceramint.2021.10.009 


 [View PDF](#) [View article](#) [View in Scopus](#)  [Google Scholar](#) 

- [115] J. Zheng, W. Zhou, Y. Ma, H. Jin, L. Guo
Combustion synthesis of $\text{LiNi}_{1/3}\text{Co}_{1/3}\text{Mn}_{1/3}\text{O}_2$ powders with enhanced electrochemical performance in LIBs

J. Alloys Compd., 635 (2015), pp. 207-212, 10.1016/j.jallcom.2015.02.114 


 [View PDF](#) [View article](#) [View in Scopus](#)  [Google Scholar](#) 

- [116] K. Elong, M. Firdaus Kasim, A. Azahidi, Z. Osman
 $\text{LiNi}_{0.3}\text{Mn}_{0.3}\text{Co}_{0.3}\text{O}_2$ (NMC 111) cathode material synthesized via combustion Method: effect of combustion fuel on Structure, morphology and their electrochemical performances

Mater Today Proc (2023), 10.1016/j.matpr.2023.02.283 

[Google Scholar](#) 

- [117] W.A.H. Wan Azizan, M.F. Kasim, K. Elong, R. Rusdi, R. Mohd Rosnan, N. Kamarulzaman
Effects of Al-dopant at Ni or Co sites in $\text{LiNi}_{0.6}\text{Co}_{0.3}\text{Ti}_{0.1}\text{O}_2$ on interlayer slabs (Li-O) and intralayer slabs (TM-O) and their influence on the electrochemical performance of cathode materials

RSC Adv., 10 (2020), pp. 40291-40299, 10.1039/d0ra07434a 

[View in Scopus](#)  [Google Scholar](#) 

- [118] T.E. Conry, A. Mehta, J. Cabana, M.M. Doeff
Structural underpinnings of the enhanced cycling stability upon Al-substitution in $\text{LiNi}_{0.45}\text{Mn}_{0.45}\text{Co}_{0.1}\text{Al}_y\text{O}_2$ positive electrode materials

Chem. Mater., 24 (2012), pp. 3307-3317, 10.1021/cm3011937 ↗

[View in Scopus ↗](#) [Google Scholar ↗](#)

- [119] M.F. Kasim, W.A.H.W. Azizan, K.A. Elong, N. Kamarudin, M.K. Yaakob, N. Badar
Enhancing the structural stability and capacity retention of Ni-rich
LiNi_{0.7}Co_{0.3}O₂ cathode materials via Ti doping for rechargeable Li-ion
batteries: experimental and computational approaches

J. Alloys Compd., 888 (2021), Article 161559, 10.1016/j.jallcom.2021.161559 ↗

 [View PDF](#) [View article](#) [View in Scopus ↗](#) [Google Scholar ↗](#)

- [120] J. Guo, W. Li
Synthesis of single-crystal LiNi_{0.7}Co_{0.15}Mn_{0.15}O₂ Materials for Li-ion
batteries by a sol-gel method

ACS Appl. Energy Mater., 5 (2022), pp. 397-406, 10.1021/acsaem.1c02939 ↗

[View in Scopus ↗](#) [Google Scholar ↗](#)

- [121] X. Tan, M. Zhang, D. Zhang, Y. Yan, Y. Wang, Z. Li
Inhibited intracrystalline cracks and enhanced electrochemical properties of
NCM811 cathode materials coated by EPS

Ceram. Int., 47 (2021), pp. 32710-32719, 10.1016/j.ceramint.2021.08.167 ↗

 [View PDF](#) [View article](#) [View in Scopus ↗](#) [Google Scholar ↗](#)

- [122] Y. Koshika, H. Kaneda, S. Yoshio, Y. Furuichi
Precursor morphology control and electrochemical properties of
LiNi_{0.35}Mn_{0.30}Co_{0.35}O₂ as a Li-ion battery positive electrode material

ACS Appl. Energy Mater., 5 (2022), pp. 8169-8177, 10.1021/acsaem.2c00698 ↗

[View in Scopus ↗](#) [Google Scholar ↗](#)

Cited by (0)

© 2023 The Authors. Published by Elsevier Ltd.



All content on this site: Copyright © 2024 Elsevier B.V., its licensors, and contributors. All rights are reserved, including those for text and data mining, AI training, and similar technologies. For all open access content, the Creative Commons licensing terms apply.

